# Characterization of White Light Emitting CdSe Quantum Dots

A thesis Submitted

To the College of Graduate Studies and Research

in Partial Fulfillment of the Requirements

for the Degree of Master of Science

in the Department of Chemistry

University of Saskatchewan

by

Jing Wang

Department of Chemistry

University of Saskatchewan

## PERMISSION TO USE

In presenting this thesis in partial fulfillment of the requirements for a postgraduate degree from University of Saskatchewan, it is agreed that the Libraries of this University may make it freely available for inspection. Permission for copying of this thesis in any manner, in whole or in part, for scholarly purposes may be granted by the professors who supervised this thesis work or, in their absence, by the Head of the Department of Chemistry or the Dean of the College of Graduate Studies and Research at the University of Saskatchewan. Any copying, publication, or use of this thesis, or parts thereof, for financial gain without the written permission of the author is strictly prohibited. Proper recognition shall be given to the author and to the University of Saskatchewan in any scholarly use which may be made of any material in this thesis.

Request for permission to copy or to make any other use of material in this thesis in whole or part should be addressed to:

Head of the Department of Chemistry

University of Saskatchewan

110 Science Place, Saskatoon, S7N 5C9

Saskatchewan, Canada

# ABSTRACT

A novel type of white light emitting semiconductor quantum dot was characterized at the ensemble and single-molecule level. This kind of semiconductor nanocrystal can be made into white light emitting diodes, which have the potential to replace conventional lighting sources. The quantum dots used in this thesis consisted of a cadmium selenide (CdSe) core, capped with ZnS, and have a surface polymer coating of poly(acrylic acid) (PAA). We have characterized the quantum dot size distribution by using dynamic light scattering (DLS), transmission electron microscopy (TEM), atomic force microscopy (AFM) and UV-Vis spectroscopy. Based on these measurements, it is clear that the white quantum dots are polydisperse, with a core size of 2.4 ± 0.5 nm, though the polymer coating swells considerably in aqueous solution. In order to explore the optical properties, the absorption and emission spectra of the ensemble quantum dots solution were measured and compared to "standard" commercial quantum dots. The emission spectrum of the white quantum dots showed two peaks, a strong blue emission peak and a weaker red emission peak. The fluorescence quantum yield of the white quantum dots was found to be less than that of commercial quantum dots. To explore the behavior of individual quantum dots, spatially-resolved single-molecule images were obtained by a dual-view single molecule fluorescence microscopy with a beam splitter which can separate the emission into red and blue components. It was found that individual white CdSe nanocrystals have a broad emission spectrum and the samples did not consist of a mixed population of red emitters and blue emitters. These results suggest that these white light emitting quantum dots can be used for pure white light LEDs and are a good candidate for the replacement for conventional lighting sources.

# ACKNOWLEDGEMENTS

First of all, I would like to extend my sincere gratitude to my supervisor, Professor Matthew F. Paige, Department of Chemistry, University of Saskatchewan, for his instructive advice and useful suggestions on my thesis. His patience and consistent encouragement helped me get through all the stages of this work. I am deeply grateful of his help in the completion of this thesis.

My heartfelt thanks also go to my committee member, Professor Robert Scott, for his valuable suggestions and advice. I further would like to thank Professor Tim Kelly and Professor Ron Steer for their advice and giving me the permission to use instrumental facilities in their labs. I thank Dr. Guosheng Liu for his help of transmission electron microscopy.

I would also like to express my thanks to our research group Connie, Hessam, Neeraj for their cooperation. I am also thankful to Brook for his help.

Last my thanks would go to my family for their support and encouragement all through these years. I also thank my friends and my fellow classmates who gave me their help and time in helping me work out my problems.

# Table of Contents

# List of Tables

# List of Figures

# List of Abbreviations

| | |
|---|---|
| AFM | atomic force microscopy |
| CCD | charge coupled device |
| DLS | dynamic light scattering |
| DSSC | dye-sensitized solar cell |
| EQE | external quantum efficiency |
| HDA | hexadecylamine |
| HOMO | Highest Occupied Molecular Orbital |
| IC | internal conversion |
| ISC | intersystem crossing |
| IVR | intramolecular vibrational redistribution |
| LED | light emitting diode |
| LUMO | Lowest Unoccupied Molecular Orbital |
| MW | molecular weight |
| OLED | organic light emitting diode |
| PAA | poly(acrylic acid) |
| PDI | polydispersity index |
| PL | photoluminescence |
| PMM | potential-morphing method |
| QD | quantum dot |
| QLED | quantum dot light emitting diode |
| R6G | rhodamine 6G |
| SBR | signal-to-background ratio |

| | |
|---|---|
| SM | single molecule |
| SMS | single molecule spectroscopy |
| SNR | signal-to-noise ratio |
| TEM | transmission electron microscopy |
| 3D | three dimension |
| 3-MPA | 3-mercaptopropionic acid |

# 1 INTRODUCTION

## 1.1 Quantum dots

Quantum dots (QDs) are nanoscale semiconductor particles that have been widely used for a number of applications. QDs exhibit a size tunable, narrow emission spectrum (the emission peak shifts towards to the red with increasing particle size), brighter emission than organic dyes, a broad excitation spectrum and excellent photostability.[1,2] Moreover, they can absorb and emit photons ranging from the UV to IR. These properties, combined with biocompatible coatings, have made them useful for a host of applications including optoelectronics, spectroscopy and biological imaging.

### 1.1.1 Quantum confinement

When a quantum dot absorbs a photon of sufficient energy, an electron will be excited into its conduction band leaving a hole in its valence band. As the size of a QD decreases, eventually the particle radius is smaller than the Bohr exciton radius (the distance between the electron and hole), which results in a spectroscopic effect called quantum confinement. In this effect, the exciton (a pair of photoexcited electron and hole) is confined to a small space (a three dimension (3D) box), on the order of the material's exciton Bohr radius. The presence of Coulombic attraction between the electron and hole prevents them from fully separating. Energy levels become discrete and quantized, and the band gap is increased relative to a bulk semiconductor. Based on the Brus equation,[3] the energy gap between the lowest level of the conduction band (so called Lowest Unoccupied Molecular Orbital (LUMO)) and the highest level of the valence band (so called Highest Occupied Molecular Orbital (HOMO)) can be approximately calculated by equation 1.1:

$$E(r)=E_{gap}+\left[\frac{h^2}{8r^2}\left(\frac{1}{m_e^*}+\frac{1}{m_h^*}\right)\right]-E_c \qquad (1.1)$$

where $E_{gap}$ is the band gap energy of bulk material, $m_e^*$ and $m_h^*$ are the effective mass of the excited electron and hole, h is the Planck constant, r is the radius of the quantum dot and $E_c$ is energy of Coulombic attraction. Due to the complicated band structures of semiconductors, the simplest way to estimate the band gap energy is to use an effective mass of electron or hole which is obtained by fitting the band structures by parabolas near the bottom of the conduction band or the top of the valance band. In the effective mass approximation model, there are some important parameters which are not taken into consideration, such as size dependent structural lattice rearrangements and surface states,[3] so it cannot predict and explain experimental results of very small quantum dots effectively. To overcome these problems, alternative models have been post developed, such as the potential-morphing method (PMM) by Baskoutas et al.[4] As the size of the quantum dots decreases, the band gap gets larger and both the optical absorption and emission bands are blue-shifted.[5]

### 1.1.2 Applications of quantum dots

In the last 20 years, quantum dots have been used in biology and optoelectronics. In biology, luminescent semiconductor quantum dots have been attached to appropriate ligands for use in biological sensing, labelling and imaging.[6,7] The main use for quantum dots is fluorescence resonance energy transfer analysis and single-particle tracking which is popular in the field of diagnosis and treatment of diseases due to rapid and sensitive detection.[8,9] Because of their small size and photostability, QDs can be used in cells for longer times than organic dyes and can enter into live cells to interact with DNA and proteins. There has been interest in detection of cancer cells by detection of QDs binding to altered DNA sequences or proteins that are present in

certain types of cancer.[10] Moreover, QDs have found application in multiple-color imaging of live cells without any effect on normal growth and development due to the narrow and tunable emission spectra.[11]

In optoelectronics, the broad excitation band of QDs has allowed them to be used in solar cells, while the narrow emission spectra have given rise to the idea that quantum dots can be made into light emitting diodes (LEDs), with the color of the LEDs being tunable through controlling the quantum dot size.[12,13] Recently, there has been interest in the development of white light emitting diodes made of semiconductor nanocrystals which has the potential to replace conventional lighting. Incandescent lamps and linear fluorescent lights are the two main light sources for the residential and commercial sectors, and high intensity discharge lighting can be found in outdoor facilities. In 2010, all of these lamps consumed nearly 700 TWh of electricity in the United States.[14] Therefore, improving energy efficiency has become an important topic and LED-based lighting is an excellent option. At the early stages of LED technology, LEDs were used in illuminated signs or traffic lights and they are now widely used in television backlight units. A report provided by the U.S. Department of Energy has indicated that LED lighting would save 300 TWh of electricity and reduce the amount of carbon emissions in the U.S. once the properties of LEDs achieve expectations.[14] The main challenge for the energy saving devices is the high cost of fabrication. This could be achieved by simplifying the design of the structures and improving the emitting materials. Compared with phosphor-converting LEDs based on GaN, one of the earlier LED technologies, organic light emitting devices (OLEDs) can be flexible and fabricated into large area with low-cost fabrication techniques such as evaporation and spin-casting due to the solution-based emitting materials.[15] At present, the best OLEDs can have a quantum efficiency of up to 20% which is much higher

than that of QLEDs.[16] The low emission efficiency of QLEDs can be attributed to the poor injection of holes into the quantum dot layer.[17] However, QLEDs have developed quickly in the past 10 years. Changhee Lee and his research group have improved the quantum efficiency of QLEDs to around 5% and the longevity has also been enhanced by introducing a new inverted structure of QLED.[18] While QLEDs have not yet matched the performance of OLEDs, their unique optical properties, such as their color stability, easily tunable color and long lifetime, still make them good candidates for LEDs. Colloidal CdSe/ZnS core-shell QDs have been the most widely investigated materials for these applications because of their high quantum yield and high photostability at room temperature.[12]

White emitting QD samples have been reported previously in the literature and generally there are three possible mechanisms by which these systems emit white light. The first is that white emission results from intermixing of red, green, blue emitting quantum dots that have narrow emission spectra. The broad spectrum can be easily adjusted by changing the ratio of different color QDs.[19] This approach has been widely used in preparing commercial LEDs. However, they still suffer from a loss in total device efficiency. Because the drying process on the substrate has driven the quantum dots in close proximity, exciton energy can be transferred from higher energy QDs to lower energy QDs through resonant energy transfer. In this case, a higher concentration and efficiency of blue emission QDs are necessary.[19] Because of the high surface-to-volume ratio of small QDs, several deep trap states can be found between the conduction band and the valence band. Once the diameter of the QDs is less than 2 nm, which is often referred as ultrasmall QDs, three distinct peaks are typically observed in the emission spectrum which arise from different trap states on its surface.[20] Such trap states typically result from surface passivating ligands or missing surface Se and Cd atoms (defects). Because of these

trap states, the emission spectrum is generally more broad.[20,21] In the final case, white emission can be achieved by exchanging the surface ligands attached to small QDs. Kamat and his group have reported that the broadening of the emission spectrum can be adjusted by addition of different concentration of 3-mercaptopropionic acid (3-MPA).[22] The band gap emission decreases, while the deep trap emission increases with the increase of the concentration of 3-MPA which results in emission of white light.

## 1.2 Fluorescence

### 1.2.1 Jablonski diagram

Fluorescence refers to the emission of light at longer wavelengths after the absorption of a light at a given shorter wavelength. When a molecule absorbs a photon, it will be excited from the ground state ($S_0$) into a higher electronic excited state $S_n$ ($n \geqslant 1$), usually the $S_1$ state. The excited molecule will relax back to the ground state by a number of pathways. A Jablonski diagram (Figure 1.1) illustrates the various processes involved in the creation of an excited exciton and the following relaxation by either non-radiative or radiative decay. The radiative decay between states of the same electron spin multiplicity (from $S_1$ to $S_0$) is called fluorescence emission. The other radiative decay between states of different electron spin multiplicity (from the $T_1$ to $S_0$) is called phosphorescence. There are also a number of other possible occurrences referred to as non-radiative processes. There are three kinds of non-radiative processes: internal conversion (IC), intersystem crossing (ISC) and intramolecular vibrational redistribution (IVR). Internal conversion occurs between energy states of the same spin multiplicity. Intersystem crossing occurs between different spin states. Vibrational relaxation is the most common non-radiative process which occurs quickly for most molecules. In this process, any vibrational state

that is selectively populated at energy higher than the average vibrational energy of the surrounding medium will undergo vibrational relaxation.

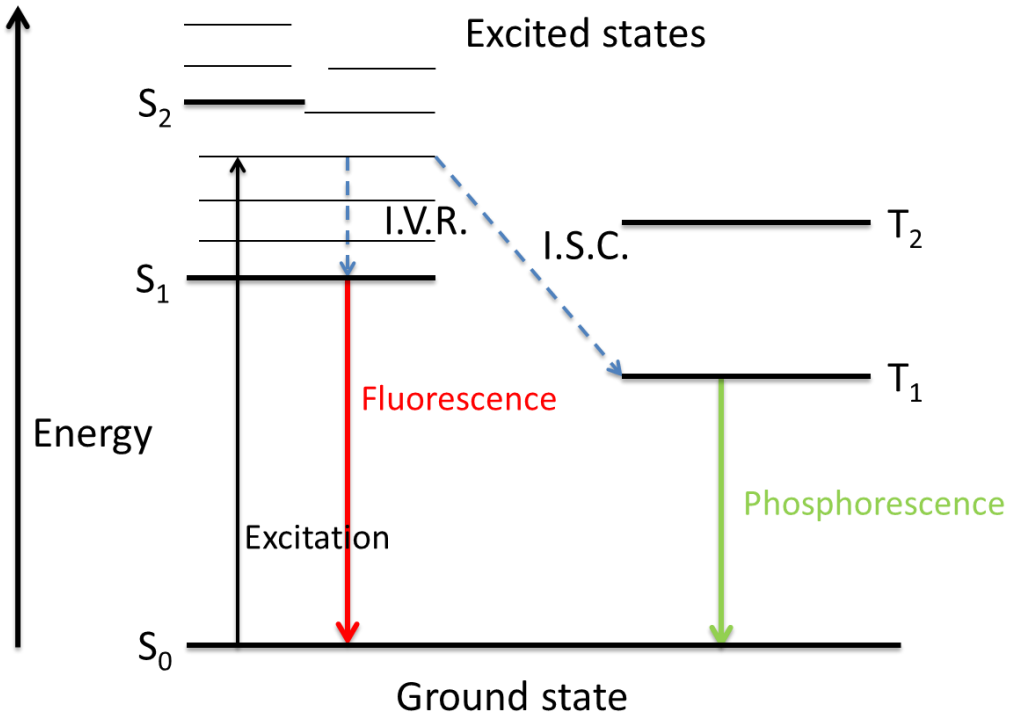


Figure 1.1 Jablonski diagram illustrating possible outcomes of a photoexcited molecule.

It is worthwhile noticing that the energy of the emitted fluorescence photon is usually smaller than the excitation photon. This can be attributed to the energy loss during the internal conversion (IC) process and intramolecular vibrational redistribution (IVR) process, when energy is dissipated during the excited state lifetime. As a result, a difference in energy can be observed by a spectral red shift of the fluorescence emission spectrum in comparison to the absorption spectrum, which is known as the Stokes shift (Figure 1.2). The extent of Stokes shift is highly dependent on the electron configuration of the excited state as well as the local

environment of the fluorescence emission. The Stokes shift of ultrasmall QDs whose diameter is less than 2 nm is usually greater than 20 nm compared to larger nanocrystals.[23]

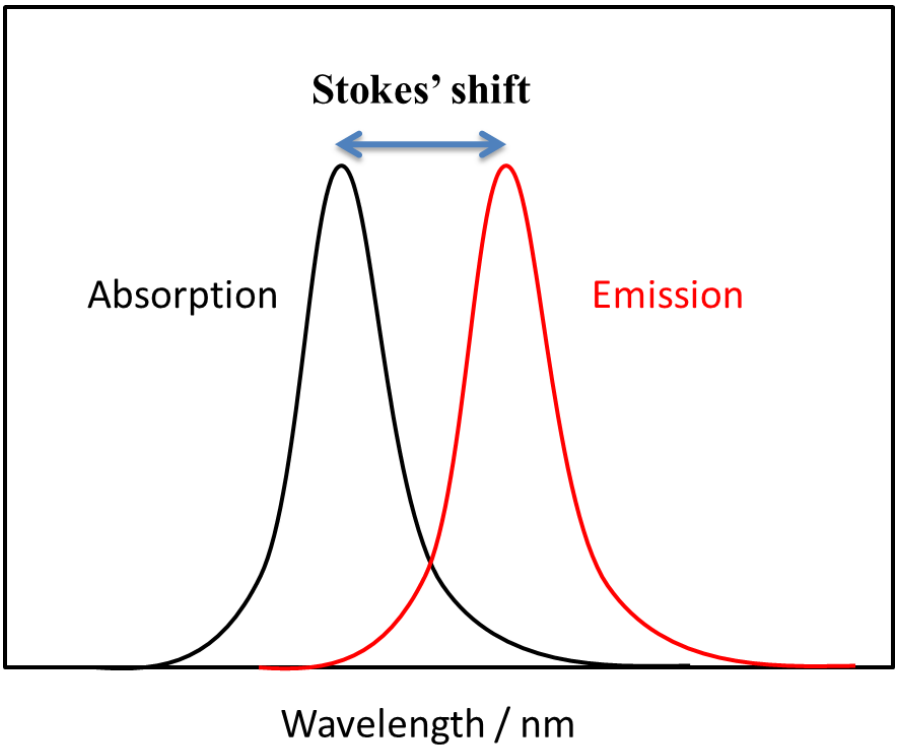


Figure 1.2 Absorption and emission spectra

### 1.2.2 Semiconductor Fluorescence

Semiconductors are defined to have conductivity between an insulator and a conductor, as shown in Figure 1.3. Conductors and insulators both have their uses, but semiconductors have remarkable properties that make them very suitable for a wide variety of applications. The optical properties of a semiconductor are controlled by its band gap between the conduction band (the lowest unoccupied band) and valence band (the highest occupied band).[24] The valence band

energy states are completely occupied in the absence of any excitation (optical or thermal). Conduction only occurs when an electron is excited across the band gap into the conduction band.

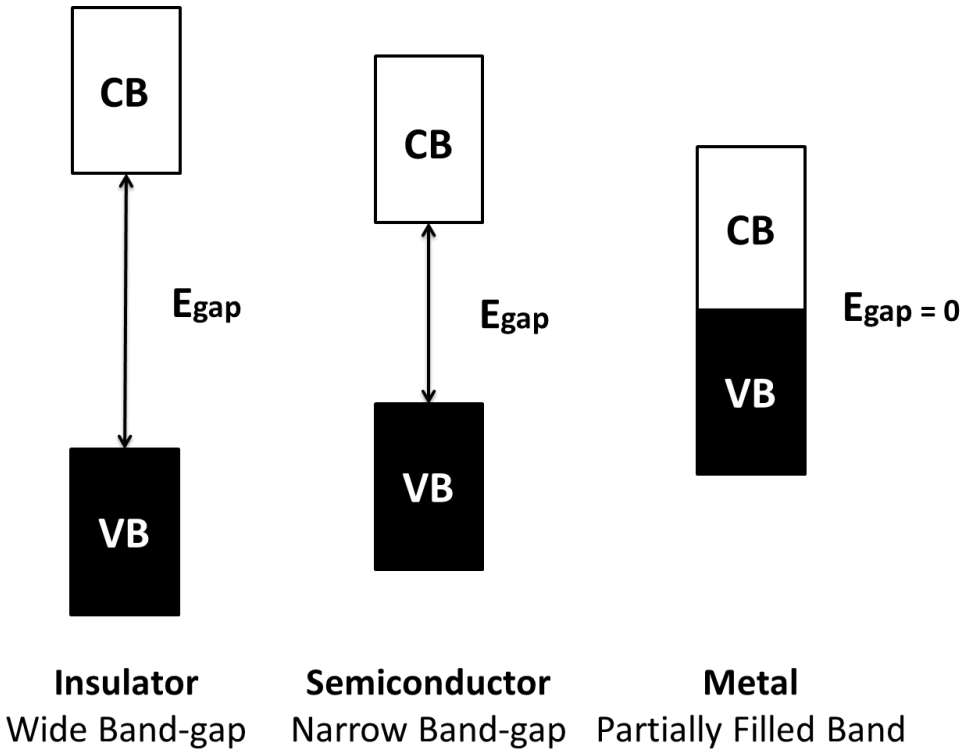


Figure 1.3 Energy band gaps of three different kinds of materials.

Semiconductor fluorescence is analogous to molecular fluorescence. In a semiconductor, an electron absorbs enough energy to jump to the conduction band leaving a hole in the valance band. Eventually they reach each other, forming an exciton which is the combination of an excited electron and a hole by Coulomb attraction. The exciton can then recombine and emit a photon. However, the electron-hole in the semiconductor may get trapped in the trap states and recombine to emit a photon with lower energy (Figure 1.4). These trap states result from several factors, including defects that are localized states in a semiconductor due to imperfections in the crystal, missing or extra atoms and dangling bonds.[25] In order to prevent the electron or hole

from getting trapped, QDs cores are usually overcoated with a wider band gap material such as ZnS or CdS. The shell reduces the number of trap states, confines the electron and hole away from the surface and suppresses broad deep trap emission. Finally, a layer of organic polymer is put on the surface, which is used to further passivate the surface, prevent the aggregation of particles and make them soluble in different solvents. According to Bowers, [21,26] the number of trap states increases with a reduction of the diameter of the quantum dot due to the increased surface-to-volume ratio and the reduced distance for the hole or electron to the surface. The deep trap emission of ultrasmall QDs gives rise to a broad emission spectrum which can be considered white light.

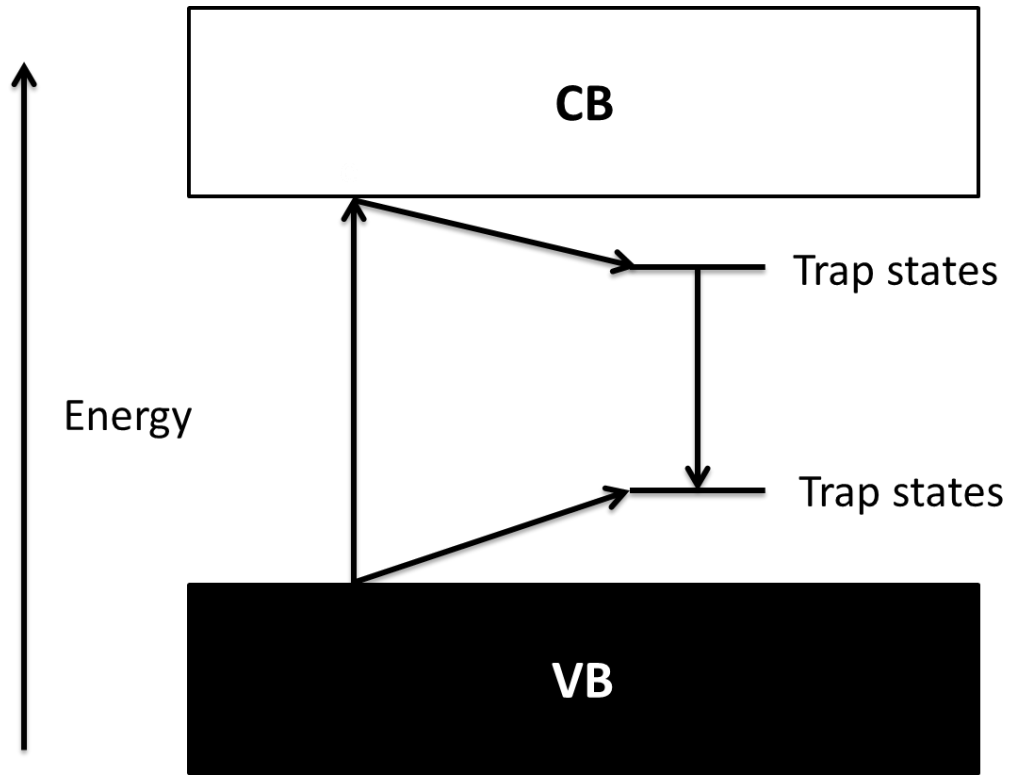


Figure 1.4 Energy description of semiconductor excitation and trap states.

## 1.3 Single molecule (SM) microscopy

Single molecule studies can be used to identify individual contributions to an ensemble average. More information can be gathered from the distribution of single molecule properties than that of averaged ensemble values. Single molecule spectroscopy (SMS) is a new field of research in which the spectroscopic properties of individual, isolated molecules are measured. Detection of a single molecule sets the limit of ultimate molecular detection at $1.66 \times 10^{-24}$ moles of molecule i.e. the inverse of Avogadro's number.[27] During single molecule fluorescence measurements, the fluorophore will be excited by a photon from the ground state ($S_0$) to the excited state ($S_1$) and emit fluorescence photons, relaxing back to the ground state. The photons can be collected by an ultra-sensitive detector, and under appropriate conditions, individual molecules can be detected above a dark background. Individual QDs can also be detected using the same approach.

### 1.3.1 Absorption cross section

Absorption cross section can be used to describe the probability that a photon of a particular wavelength passing through a molecule will be absorbed by the molecule.[27] A high absorption cross section results in a high probability of photon absorption and thus is important for achieving strong fluorescence emission. The absorption cross section of a randomly oriented molecule can be calculated by the following equation:

$$\sigma_p = 2\pi\left(\frac{\lambda}{2\pi}\right)^2 \left(\frac{\gamma_r}{\Gamma_{tot}}\right) \qquad (1.2)$$

where $\lambda$ is the light wavelength, $\gamma_r$ the spontaneous fluorescence rate, and $\Gamma_{tot}$ the total frequency width of the absorption.

A simple way to determine the absorption cross section (in unit of $cm^2$) of the molecule at room temperature is through the equation:

$$\sigma_p = \frac{2.303\varepsilon}{N_A} \qquad (1.3)$$

where ε is the molar extinction coefficient (in L $mol^{-1}$ $cm^{-1}$) at the desired wavelength and $N_A$ is the Avogadro constant. The emission rate from a fluorophore will increase with increasing excitation intensity before the molecule is optically saturated. Optical saturation occurring at very high excitation intensity limits the emission because of a decrease in an absorption cross section area and increase in the background signal.[27] Therefore, optimization of the excitation power is crucial for the measurement of individual molecules. With sufficiently high excitation power, the total number of emitted photons will also be limited by the occurrence of photobleaching, which will stop the fluorophore from absorbing and emitting photons. The reason for the photobleaching is complicated and remains unclear. Photo-oxidation is generally believed to be one of the main causes of photobleaching.[28] Reducing the amount of oxygen a sample is exposed to generally helps to postpone the occurrence of photobleaching. Because of optical saturation and photobleaching, the signal size we get from the fluorescence emission is usually smaller than the ideal model.

### 1.3.2 Quantum yield

As shown in Figure 1.1, an excited fluorophore will relax back to the ground state via either radiative or non-radiative decay process. Fluorescence quantum yield ($\phi_F$) is defined as the ratio of the number of photons emitted by the molecule to the number of photon absorbed, which is given by:

$$\Phi_F = \frac{k_{rad}}{k_{rad} + k_{nr}} \qquad (1.4)$$

where $k_{rad}$ and $k_{nr}$ represent the radiative and non-radiative rate constants respectively. For single photon absorption events, the sum of the quantum yields of all parallel relaxation processes involving radiative and non-radiative decay must equal 1. Therefore molecules with a high fluorescence quantum yield, as close to unity as possible, are preferred in single molecule fluorescence spectroscopy studies. The easiest way to estimate the quantum yield of a fluorophore is by comparison with standards of known quantum yield (usually highly fluorescent molecules with $\phi_f$ near 1).[29] Rhodamine 6G which exhibits a $\phi_f$ value of greater than 0.9 is one of the ideal standards.

### 1.3.3 Signal-to-noise and signal-to-background issues

Signal-to-noise ratio (SNR) and signal-to-background ratio (SBR) are two of the most important factors which decide whether a single molecule can be measured. In the narrow sense, the word "noise" refers to fluctuations which contain unwanted information. Some sources of noise can be minimized, while some of them will be always present, such as shot noise of any detected photons and dark counts from the photodetector.[30] Background is usually derived from the fluorescence emitted by contaminated solvent or substrates and optical parts in the setup, which can be minimized by using ultrapure solvent or ultraclean substrates.[27] Figure 1.5 demonstrates that the signal of a detector is generally made of the detector offset and dark counts, the background and the signal which contains information of interest. The dark count refers to the reading of the photo detector in the absence of excitation light source, and it does not vary according to the incident power. The scale of background is usually proportional to the power of excitation which is similar to the signal of interest.

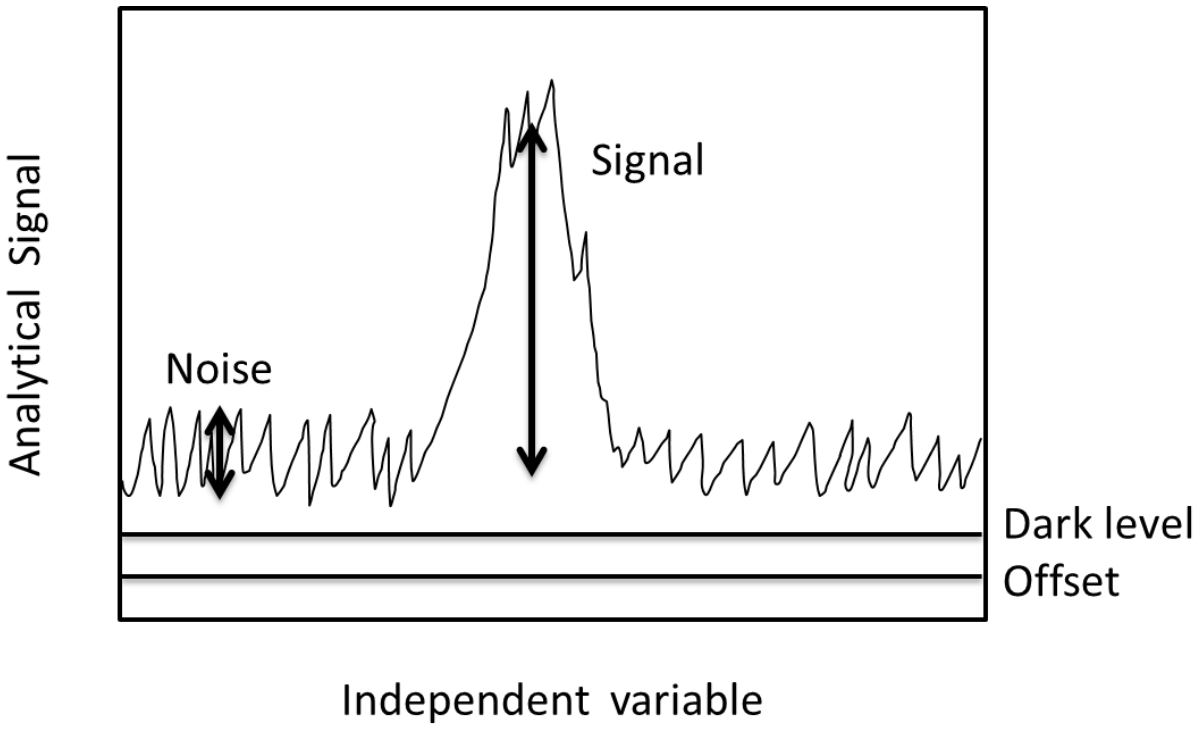


Figure 1.5 Definitions of the offset, dark level, noise and signal from a single molecule.

As mentioned, the background may result from both experimental sources which include colored glass filters and the microscope objective itself and sample preparation. The background photons generated from the sample itself are mainly due to the elastic Rayleigh scattering and Raman scattering. Rayleigh scattering is known as the elastic process which only alters the propagating direction of the photon without any energy loss. Raman scattering, on the other hand, involves the energy loss of the incident photon due to the interaction of the photons and molecule. This kind of light scattering results in a spectral red-shift to a longer wavelength (less energy). Since the signal of background will increase with the enhanced intensity of excitation power, using microscopy techniques with a small excitation volume helps to reduce the background and focus on the single molecule of interest. Moreover, the sample preparation for SM fluorescence microscopy is extremely demanding in comparison with the conventional bulk measurements.

Non-fluorescent immersion oils and ultrapure solvents without any fluorescent impurities must be used in order to get a very low background signal.

In addition to reducing background signals, maximizing the collected signal is also necessary in single molecule fluorescence spectroscopy experiments. SNR is defined as the ratio of the level of signal to the level of noise. Based on the assumption that the contributor to signal and noise are Poisson distributed, the SNR can be described as:

$$\mathrm{SNR} = \frac{\mathrm{S}}{\sqrt{\mathrm{S} + \mathrm{B} + \mathrm{DC}}} \qquad (1.5)$$

where S is the fluorescence signal count rate from the molecule, B is the background count rate and DC is the dark count rate from the photodetector. In order to observe the single molecule signal, the size of signal needs to be compared to the size of background and dark counts. To express this quantitatively, the SNR can be determined by all the following factors in the half-empirical equation:

$$\mathrm{SNR} = \frac{\mathrm{F}\phi_{\mathrm{F}}\left(\frac{\sigma_{\mathrm{p}}}{\mathrm{A}}\right)\left(\frac{\mathrm{P}_0}{\mathrm{h}\upsilon}\right)\mathrm{i}}{\sqrt{\left(\mathrm{F}\phi_{\mathrm{F}}\left(\frac{\sigma_{\mathrm{p}}}{\mathrm{A}}\right)\left(\frac{\mathrm{P}_0}{\mathrm{h}\upsilon}\right)\mathrm{i}\right) + \mathrm{C_b}\mathrm{P}_0\mathrm{i} + \mathrm{N_d}\mathrm{i}}} \qquad (1.6)$$

where $\phi_F$ is the fluorescence quantum yield of the molecule of interest, $\sigma_P$ is the absorption cross section, i refers to the detector counting interval, A is the beam area, $P_0/h\nu$ is the number of incident photon per second, $C_b$ is the background count rate, $N_d$ is the dark count rate and F refers to the instrument-dependent factor. The overall collection efficiency in terms of instrument-dependent factor (F) is determined by each component in the microscopic setup (shown in Equation (1.7)):

$$\mathrm{F} = \mathrm{e_{obj}} \times \mathrm{e_{opt}} \times \mathrm{e_{filter}} \times \mathrm{e_{det}} \qquad (1.7)$$

where $e_{obj}$ , $e_{opt}$, $e_{filter}$, and $e_{det}$ represent for collecting efficiency of the microscope objective, optics, filter and photodetector respectively.[27]

## 1.4 Synthesis of quantum dots

In the past two decades, several routes have been developed to synthesize QDs. The most frequently cited process of synthesizing monodisperse QDs is referred to as the hot-injection method based upon the work of Murray and co-workers in 1993.[31] A cool solution of precursor molecules is injected into a high boiling point organic solvent at high temperature under an inert gas atmosphere. This gives rise to the formation of QD nuclei and this is stopped by rapidly cooling the reaction. Growth of the existing nuclei is promoted by increasing temperature again but the solution is always kept below the nucleation temperature. The quality of the products depends on the speed of injection and how well one can control the nucleation and the growth temperatures. Under these synthetic conditions, a narrow size distribution of QDs could be achieved by the separation of nucleation and growth.

For the aim of applications in different areas, the synthesis of water-soluble QDs has become a topic of broad scientific interest. With the traditional synthesis methods, the resulting QDs can be made water soluble by replacing the hydrophobic surface ligands with hydrophilic ones or by adding an additional solubilizing layer of silica.[32-34] In these cases, the exchange of surface ligands often leads to a low stability of QDs in water and the formation of defect sites on the particle surface which results in a decrease in fluorescence quantum yield. Recently, some more direct routes to synthesize water-soluble QDs have been developed.[35,36] However, most of the existing methods required stringent control of the atmospheric conditions and high temperature. Our collaborator has developed an alternative approach for making QDs in aqueous and ambient conditions. Aqueous Cd salt solutions are mixed with poly(acrylic acid) (PAA),

leading to collapse of the extended polymer chains, and followed by photochemical cross-linking to form a nanotemplate within which the quantum dot core is grown. The synthesis uses low particle growth temperatures, which favours formation of small QDs, and uses only aqueous solutions. Chemical synthesis of the quantum dots used in this study was carried out by Dr. Jane Goh at the Department of Chemistry, University of Toronto. More details are provided in Chapter 2.

## 1.5 Research objectives

The overall object of my master's project is to determine the reason why the semiconductor quantum dots described above emit "white" fluorescence. Recently, there has been interest in the development of white light emitting diodes made of semiconductor nanocrystals for lighting applications. If these semiconductor quantum dots are to be used in the future for solid state lighting, we need to understand the mechanism responsible for the white emission. Because of the size-dependent optoelectronic properties of quantum dots, a fundamental understanding of the nanocrystal size distribution is required, which will be described in Chapter 2. This was followed by measurements conducted using conventional optical spectroscopy, including absorption spectroscopy and fluorescence spectroscopy to examine basic optical properties. Efforts were made to measure individual contributions to the average by a dual-view single molecule fluorescence microscopy (Chapter 3). Another important issue to be explored is the reproducibility of the synthesis. Another batch of white quantum dots was analyzed using all the measurements above to assess the batch-to-batch reproducibility. The results from these experiments are presented and discussed in this thesis.

# 2 Synthesis and size distribution measurements

## 2.1 Overview

Three different kinds of size distribution measurements have been carried out in order to determine the size of the QDs. The focus of this study was to determine whether the white light emission is attributed to any special size distribution. The results gathered from the three different kinds of instruments are presented and discussed in this chapter.

## 2.2 Materials and methods

### 2.2.1 Sample Preparation

The samples (white QDs solution-CdSe/ZnS-PAA and CdSe-PAA solution) were provided by Dr. Jane Goh from University of Toronto. Poly(acrylic acid) (MW ~450,000) was from Aldrich. Cadmium nitrate, sodium selenite, hydrazine and thioacetamide were from Alfa Aesar. All chemicals were used without further purification. The water used in all the experiments had a resistivity >18 MΩ/cm.

**$Cd^{2+}$-PAA**

PAA was weighed out (2.0 g) and dissolved in 1 L of water and the pH of the solution was adjusted to ~6.8 with the addition of NaOH (10 M solution), and monitored using pH paper. To this slightly viscous solution was slowly added 1 L of $Cd(NO_3)_2$ (5 mM solution) to produce a clear colorless solution, which was subsequently exposed to 254 nm light for 1 hour resulting in a pale yellow solution of viscosity similar to water. This solution was referred to as $Cd^{2+}$-PAA.

**CdSe-PAA**

To 1300 ml solution of $Cd^{2+}$-PAA in a round bottom flask were added $Na_2SeO_3$ solution (13 mL, 50 mM solution) and hydrazine (6.5 mL); this was refluxed for 2 hours. This solution was referred to as CdSe-PAA.

**Purification**

A 100 mL of the crude CdSe-PAA solution was mixed with NaCl (5 mL, 3 M solution) and shaken vigorously. To this was added 100 mL of ethanol (absolute or 95%) and then shaken vigorously. The solution was centrifuged at 12,000 RCF for 15 minutes, and then decanted. The pellet was washed with 50% ethanol three times, and air-dried overnight at room temperature. The dried pellet was reconstituted with 20 mL of $H_2O$.

**CdSe/ZnS-PAA**

To 1350 mL of $H_2O$ was added the purified CdSe-PAA solution above (150 mL), $Zn(NO_3)_2$ solution (9.75 mL, 250 mM), and thioacetamide solution (0.975 mL, 250 mM). The mixture was refluxed for 20 h.

The Lumidot CdSe/ZnS (core-shell type commercial QDs stabilized with hexadecylamine (HAD) ligand, 532 nm) in toluene was purchased from Sigma-Aldrich. Before each measurement, the white QDs were diluted in ultrapure Millipore water and commercial QDs in toluene to an appropriate concentration and filtered with a 0.2 μm syringe filter. The solution was then sonicated for 10 minutes to break up any possible aggregates. For AFM measurements, 50 μL of the diluted sample was deposited onto a freshly cleaved mica sheet (SPI supplies) and allowed to evaporate under ambient condition for 30-40 minutes depending on the density of particles required. The residual solution was dried with a stream of nitrogen gas. For TEM measurements, carbon film-coated copper grids (200 square mesh copper grids; Electron

Microscopy Sciences) were treated in a benchtop plasma cleaner (Harrick Scientific) under the "medium" power setting for about 15-30 seconds. This treatment usually makes the grids hydrophilic, and allows hydrophilic particles to spread more evenly. The sample was prepared by dropping 5 μL of the diluted solution onto a plasma treated grid and evaporated at room temperature overnight before imaging. These methods were followed for all samples.

### 2.2.2 Instrumentation

All the measurements were performed in ambient conditions. The hydrodynamic diameter was measured on a Malvern Zetasizer with a measurement angle of 173º backscatter using 10 mm x 10 mm quartz cuvettes. Samples were equilibrated for two minutes at 25 °C before a minimum of three measurements were made. Dynamic light scattering (DLS) measures the intensity fluctuations of scattered light arising from Brownian motion of particles in solution which can be converted to an intensity correlation function.[37] An important feature of Brownian motion for DLS is that small particles move quickly and large particles move more slowly. As the particles move around, the movements will cause the intensity of the scattered light to fluctuate, and the fluctuations are directly related to the rate of diffusion of the particle through the solvent.[38] The fluctuations can be measured by the detector and analyzed to determine a hydrodynamic diameter for the particles by using the Stokes-Einstein equation:

$$d_h = \frac{kT}{3\pi\eta D} \qquad (2.1)$$

where k is Boltzmann's constant, T is the temperature in K, η is the solvent viscosity and D is the diffusion constant derived from the intensity correlation function. The simplest method to analyze the intensity correlation function is the cumulants analysis which can give the average

size and the value of polydispersity index for the sample.[39] The log of the G1 correlation function can be fitted by cumulants analysis by the following equation.[40]

$$\ln[G1] = a + bt + ct^2 + dt^3 + et^4 + \cdots \qquad (2.2)$$

The polydispersity index can be calculated from two terms in the above equation.

$$PDI = \frac{2c}{b^2} \qquad (2.3)$$

where b is the Z-average diffusion coefficient. In this case, the particles are assumed to be spherical or near-spherical in shape.[41] Based on an equivalent sphere with the same diffusion coefficient, if the sample is monodisperse and can be dispersed well in the solvent, the calculated average size is acceptable. In other words, the average size might be calculated incorrectly if the distribution is very broad.[42]

AFM images were obtained using a Dimension Hybrid Nanoscope system (Veeco Metrology Group) which uses a cantilever with a sharp nanometer-sized tip to scan the specimen surface. After the tip touches the surface of the sample, the probe will experience a force between the tip and the sample which will cause bending of the cantilever. A laser beam is used to detect the cantilever bending by reflection from a mirror placed on the back of the cantilever onto a split photodiode.[43] For AFM particle analysis the size of the small particles should be greater than the topographical features of the substrate. Therefore, the ultraflat and hydrophilic properties of mica make it as an ideal substrate for AFM measurements. A schematic diagram of the system is shown in Figure 2.1.

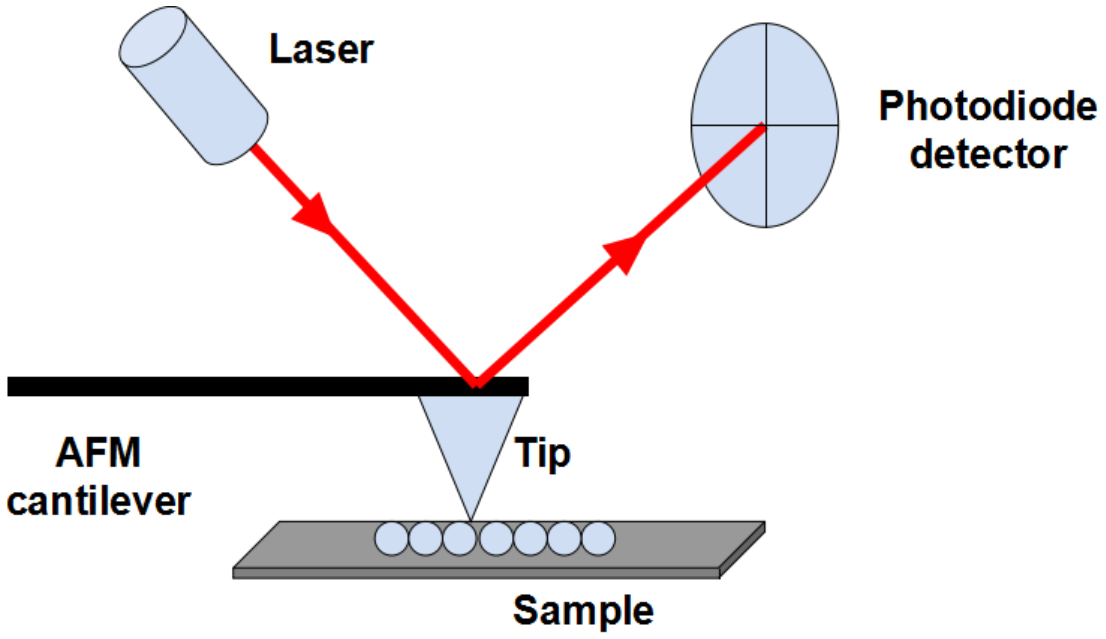


Figure 2.1 Schematic diagram of an AFM. A laser beam is focused on the back of the cantilever to measure changes in cantilever deflection. The beam is reflected into a four-quadrant photodetector.

Contact imaging mode was used to collect topographical images. Samples were typically imaged with a scan size of 2 μm x 2 μm and a scan rate of 1.00 Hz. Nanoparticle height (z direction) was used to determine nanoparticle diameter. The Z-axis resolution is usually better than the resolution in the X-Y scan plane of the sample surface, especially when the size of the probe is much larger than the surface features. Tip artifacts can make in-plane measurements (x–y direction) larger than the actual nanoparticle width which cannot be used to estimate the size of nanoparticles.[44] In the X-Y plane, we can determine whether the sample is dispersed well and find the sample texture.[45]

Transmission electron microscopy (TEM) was carried out on a Philips CM10 (1990) TEM in the Department of Biology. In TEM, a focused beam of electrons is transmitted through a specimen. After the interaction of electron beams with the sample, an image is formed from the

electrons transmitted through the specimen. Because of the much higher electron density, heavier atoms scatter more electrons and less electrons pass through. Therefore, TEM can be used to get the size of the QD cores. However, the polymer coating cannot be viewed due to the lack of scattering contrast.[46] In this thesis, TEM images were recorded at 73 k x magnification. At this level of magnification, the scale can be set as 1 mm is equal to 14 nm.

## 2.3 Results and discussion

### 2.3.1 Dynamic light scattering

The size distribution of quantum dots in water determined from DLS is shown in Figure 2.1. The intensity-weighted average particle hydrodynamic diameter (Z-average) was around 41 nm with a polydispersity index (PDI) of 0.28 which is used to describe the width of the particle size distribution.[47] Based on the algorithms described in the method section, values smaller than 0.05 indicate the sample is highly monodisperse, while values greater than 0.70 indicate the sample has a very broad size distribution.[41] The value of our sample was between 0.05 and 0.70 indicating our sample was moderately polydisperse.

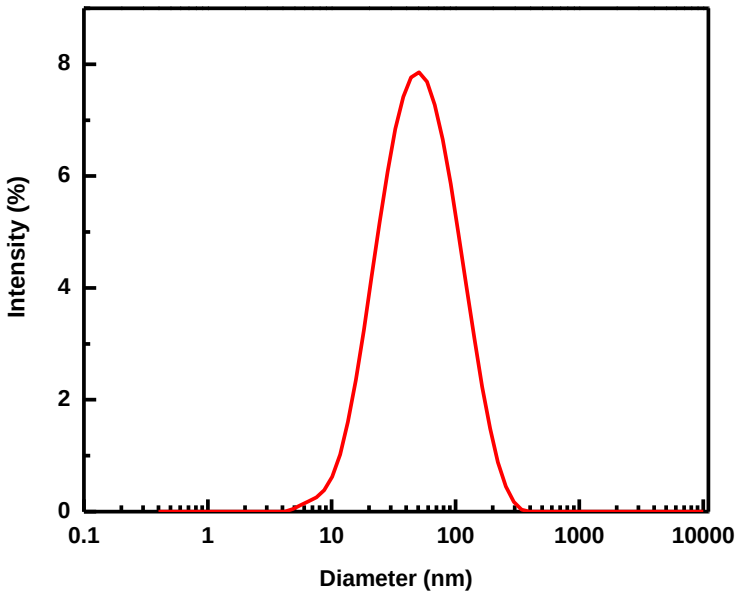


Figure 2.2 Analysis of nanocrystal size by DLS. The size distribution was shown by intensity and the Z-average diameter is 41 nm with a polydispersity index of 0.28.

As shown in Figure 2.1, the white QD solution was polydisperse with relatively high value of PDI and broad width of distribution. When a particle moves through a liquid medium, a hydrated layer will adhere to its surface which has an important effect on the movement of the particle. Thus the hydrodynamic diameter of nanoparticles gives us information of the inorganic core along with any coating material and the hydrated polymer layer as it moves under the influence of Brownian motion. As described in the procedure of synthesis, the quantum dot core was grown in a collapsed polymer (PAA) system, which acted as a nanotemplate. (Figure 2.2 (a)) Therefore, the hydrodynamic diameter of the quantum dots measured by DLS consists of CdSe core, shell of ZnS, coating material (PAA) and any additional hydration layer of water associated with the polymer shell. Based on the molecular structure of PAA (Figure 2.2 (b)), when it

dissolves in water at neutral pH, many of the side chains of PAA will lose their protons and acquire a negative charge. This gives PAA the ability to absorb protons from the environment which makes the thickness of the hydrated layer unknown. The thickness of the hydrated layer depends on various factors, such as the electrical conductivity of water and the properties of the coating material. Moreover, since the PAA is composed of many repeated subunits, it is impossible to keep the length of the each polymer and the thickness of the polymer shell constant. The unknown thickness of the hydrated layer and length of the coating polymer make the hydrodynamic diameter of quantum dots variable. As noted in the Zetasizer instrument manual, there will be some error in the conversion from intensity distribution to number distribution, especially in a polydisperse system, so the intensity-based value cannot be directly compared to a number mean value from other methods.[41] This instrument is usually used for comparative purposes and determining aggregates of the particles due to the sensitivity to the presence of aggregates.

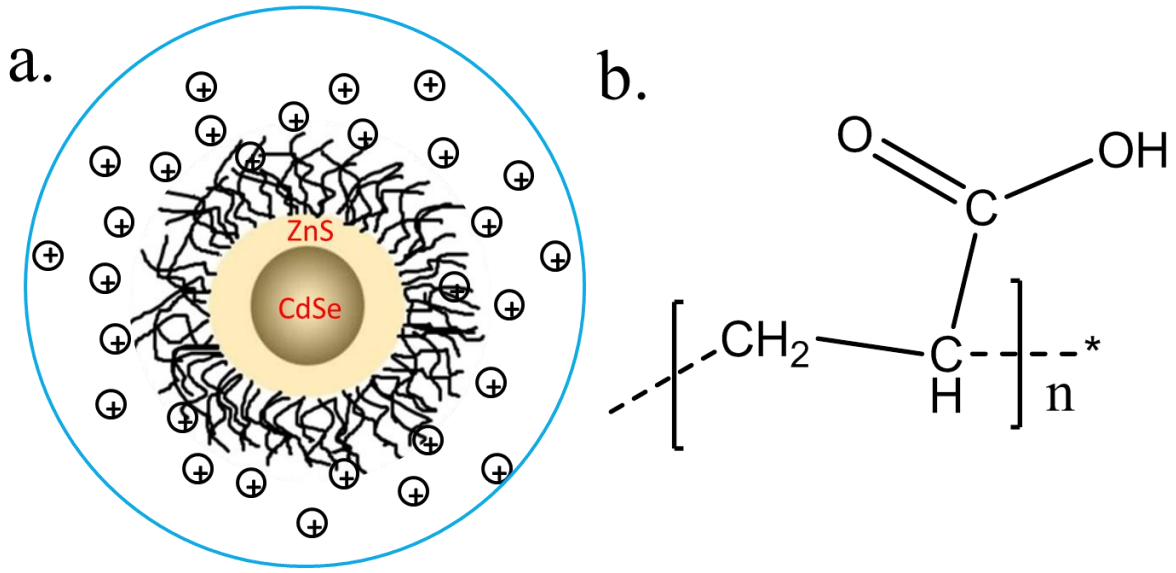


Figure 2.3 (a) Hydrodynamic diameter measured by DLS consists of quantum dot core, coating material (PAA) and a hydrated layer of the solvent. (b) The chemical structure of PAA.

### 2.3.2 Atomic force microscopy

DLS is a rapid, non-destructive and valuable technique for particle size determination in solution. It is useful for measuring size for identifying the presence of aggregates and estimating relative proportions of particles in liquid samples. A supporting measurement was performed by AFM in contact mode with quantum dot solutions deposited onto a cleaned substrate (mica) (Figure 2.3).

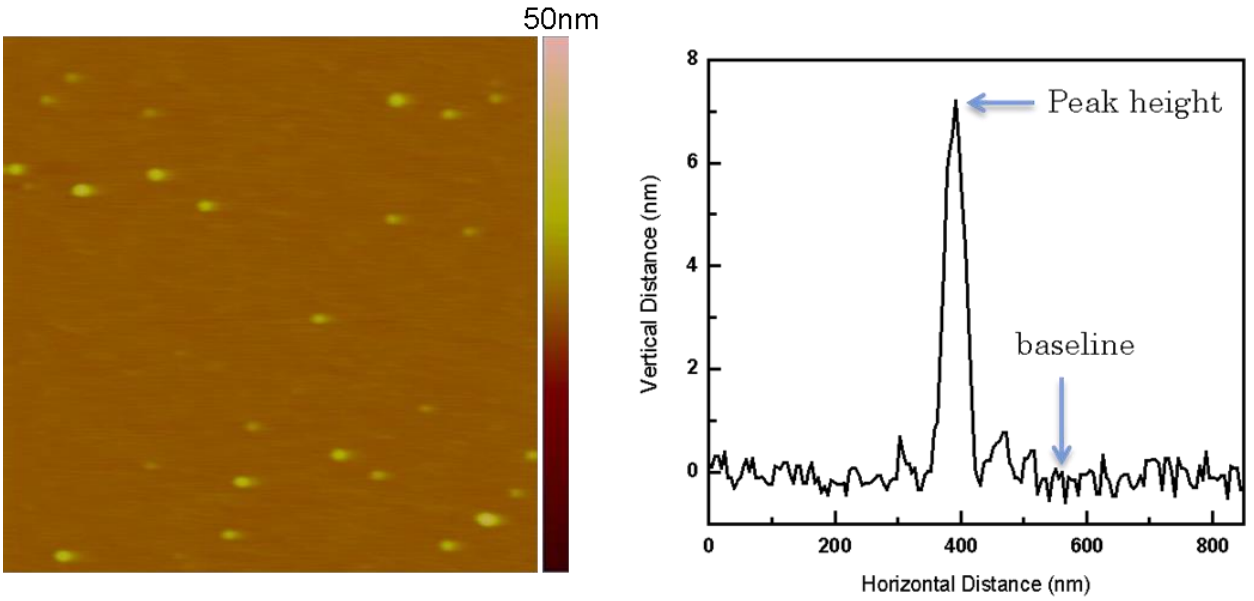


Figure 2.4 AFM height image (2 μm x 2 μm) and the cross-sectional analysis. Z-axis scale is 50 nm. The difference between the peak height and the average baseline is the particle size (diameter).

The AFM imaging indicates that quantum dots dispersed well on the substrate and it was easy to differentiate the single particles from background and aggregated particles. However, as noted previously, the core of the QDs was grown in a nanotemplate made of PAA. Therefore, the isolated spots on the substrate surface may be either polymer with CdSe cores inside or polymer without any cores, which cannot be distinguished by AFM. For small size quantum dots whose

geometry could change significantly due to tip-sample forces, the Z-axis resolution is usually better than the resolution in the X-Y scan plane of the sample surface. The particle height was measured by making several cross-sectional line profiles across the nanoparticles and subtracting the average baseline from the peak height.

For statistical study, 288 nanoparticles were measured. The histogram of particle heights (Figure 2.4) shows the majority of the quantum dots were between 2 nm and 10 nm in diameter. The AFM analysis yielded a nominal diameter of 8 nm with a standard deviation of 5 nm. The nanoparticle cores are probably less than 8 nm because of the PAA within which the crystalline nanoparticle has grown. The AFM results also suggest that the sample was polydisperse because of the wide range of the sizes, which is consistent with what was found by DLS. As noted earlier, the water soluble quantum dots are grown in a nanotemplate made of PAA and coated in a ZnS shell to make up for crystal defects. These two coats make the quantum dots thicker by an unknown radius, especially the coating polymer which was the main reason for this phenomenon. Moreover, there are also some other different reasons for polydispersity from that of DLS. Since AFM measures the sample after it was dried on the substrate, the drying process on the mica might also affect the height. The selection of substrate plays a significant role in imaging by AFM because the nature of the substrate influences the formation of nanoparticles and solvent. For example, mica, which is a very hydrophilic substrate, may cause the nanoparticles to form agglomerates and form a layer of water.[48] The nature of the nanoparticle surface also has an effect on the distribution of the particles on the substrate. When the quantum dots were dried on a substrate, the interactions between quantum dots and between a quantum dot and the substrate may cause various effects on dispersing of nanoparticles, especially during and after evaporation. Also, when the PAA dried out on the substrate, it will shrink to different sizes losing water from

the solution. It is interesting to note that the main effect is the random placement of quantum dots on the substrate and particle agglomeration.[49] Moreover, the exposure time and the dilution of the solution may cause the different formation of quantum dots.[45] All of the above possibilities result in the polydispersity measured with atomic force microscopy.

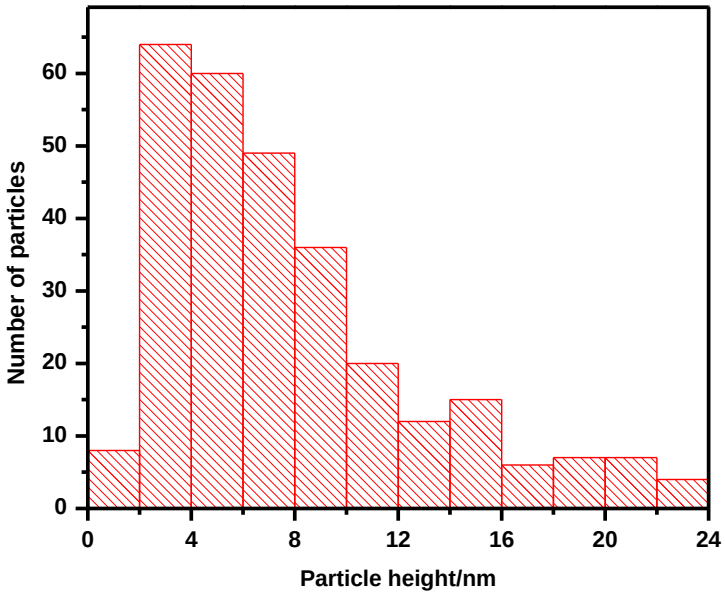


Figure 2.5 AFM size distribution data is plotted with respect to the frequency of appearance (288 quantum dots were measured). The average size was 8 ± 5 nm.

### 2.3.3 Transmission electron microscopy

TEM plays an important role in characterization of nanoparticle size distribution. To compare the white QDs with a standard QD, the size of commercial QDs in toluene was also measured by TEM under the same conditions. Figure 2.5 (a) shows a TEM image of commercial QDs. As can be seen from the image, the quantum dots dispersed well on the grid and the contrast can be used for quantitative analysis. Figure 2.5 (b) indicates the size distribution

histogram by measuring 300 particle diameters from (a). The average size was determined by fitting the size distribution to a Gaussian function (black curve) and then calculating the mean and width of the distribution. TEM measurements yielded a nominal diameter of 3.1 nm with a standard deviation of 0.5 nm. This observation is in good agreement with the size provided by the manufacturer (around 3.3 nm).

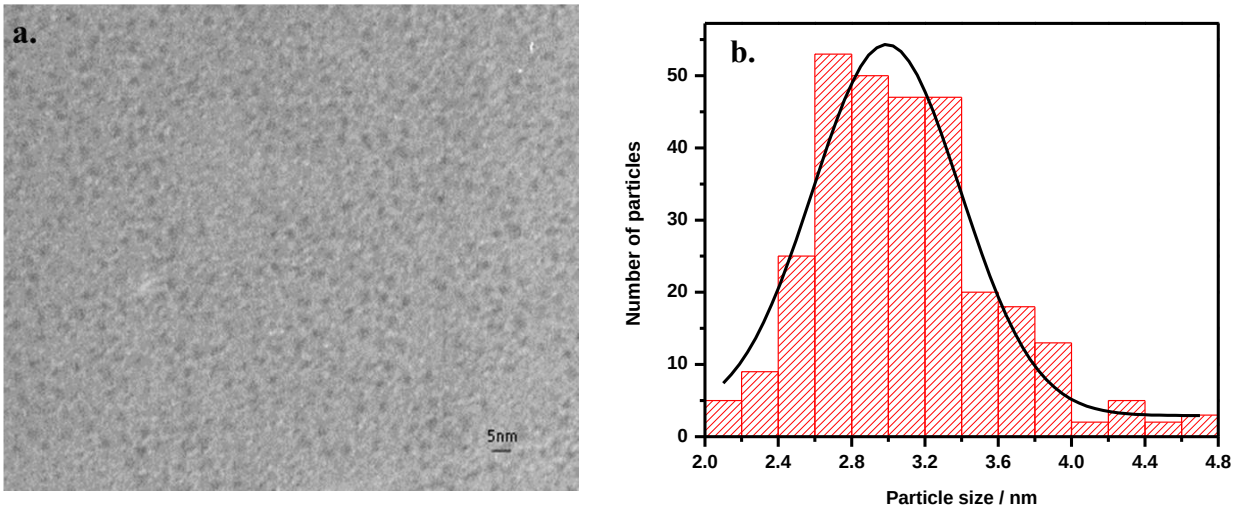


Figure 2.6 (a) TEM image of commercial QDs in toluene, (b) Size distribution histogram from (a), which was obtained by measuring 300 particles diameter. The black curve is the fitted Gaussian curve. The average core size is 3.1 ± 0.5 nm.

In order to determine the size of the core which has an effect on the optical properties, TEM was performed on the CdSe/ZnS-PAA samples and the CdSe-PAA samples. Figure 2.6 (a) shows the TEM image obtained from the CdSe/ZnS-PAA sample, while (c) shows the image of CdSe-PAA. It was found that QDs dispersed well on the grids, thus, the size and shape of the quantum dot cores can be determined. Within the resolution capabilities of the microscope, the sizes of QD before and after coating the shell of ZnS did not differ significantly from each other.

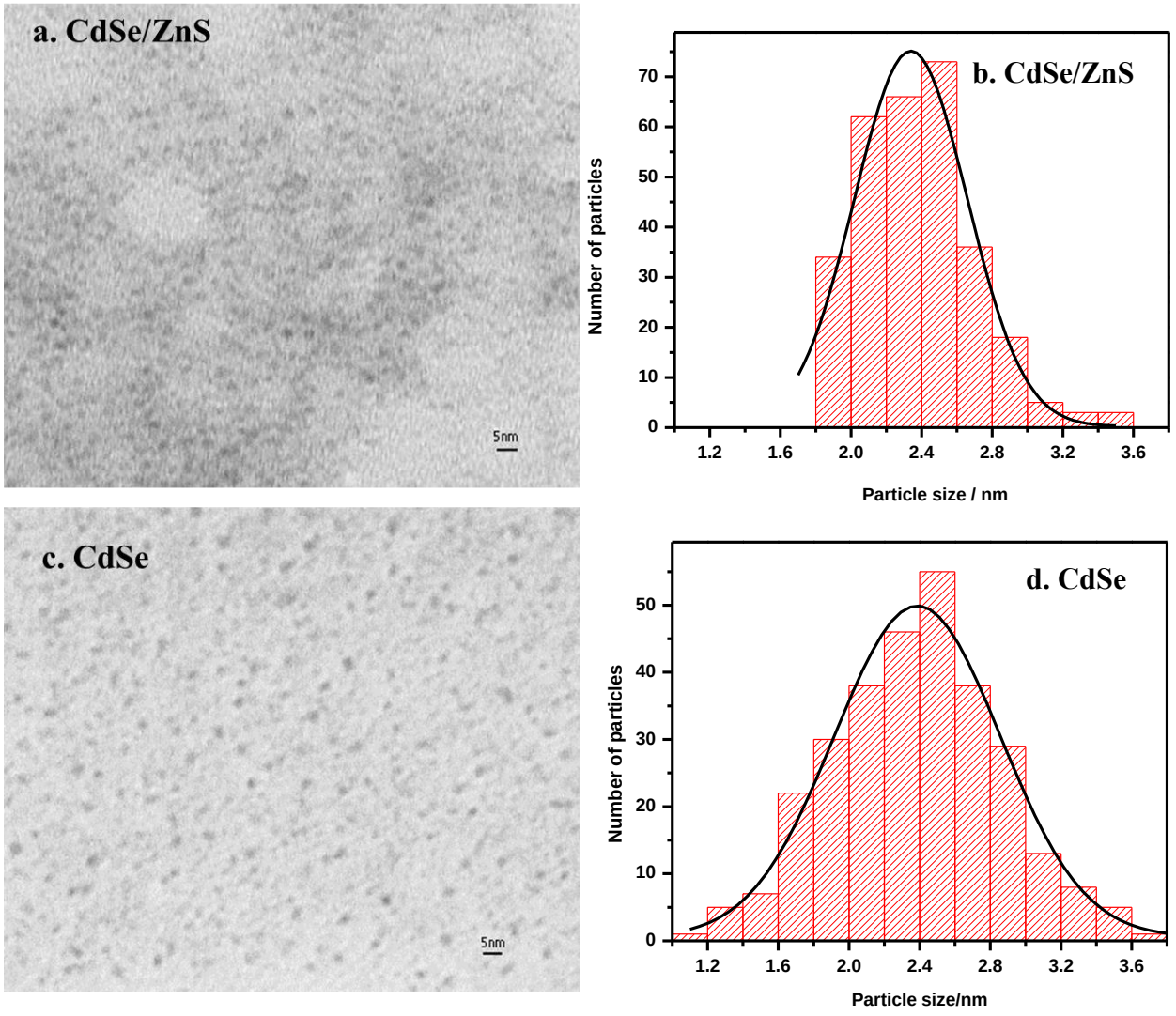


Figure 2.7 TEM images of (a) the CdSe/ZnS-PAA samples and (c) the CdSe-PAA samples. (b) (d) Size distribution histograms from (a) (c), which were obtained by measuring 300 particles diameter of each sample. The black curve is the fitted Gaussian curve. The average size of CdSe/ZnS-PAA was 2.4 ± 0.3 nm, while the average size of CdSe-PAA was 2.4 ± 0.5 nm.

To compare the sizes of both sets of QD quantitatively, the statistical results from analyzing Figure 2.7 (a) and (c) are shown in (b) and (d), respectively. The size distribution histograms were obtained by measuring 300 particle diameters of each sample. We also fitted the size

distribution by a Gaussian curve (black curve) and then calculated the average size. The average size of CdSe-PAA was 2.4 nm with a standard deviation of 0.3 nm, while the average size of CdSe/ZnS-PAA was also 2.4 nm with a different standard deviation of 0.5 nm. Since PAA consists of C atoms, H atoms and O atoms which have low electron density, it would not be visible by TEM. The shell of ZnS with high electron density should be visible, so it was expected that the QD with the shell should be larger than that of the QD without the shell. However, the result turned to be different from expected. This observation can be attributed to the thin layer of ZnS which is difficult to be viewed by low-resolution TEM. It is worth noting that the size of our white QD is smaller that of commercial one which results in the differences of optical properties due to quantum confinement.

## 2.4 Conclusions

The size distribution of quantum dot samples prepared by our collaborators has been measured with by three different technique, namely dynamic light scattering (DLS), atomic force microscopy (AFM) and transmission electron microscopy (TEM). DLS is a rapid, non-destructive and valuable technique for particle size determination, which gives information of hydrodynamic diameter of the nanoparticles in liquid samples. (Figure 2.8) Compared with the average size of AFM or TEM, the average size of DLS was much larger (shown as the blue circle). Also, in a water solution at neutral pH, PAA is an anionic polymer, which makes PAAs have the ability to absorb a large amount of water and swell to many times their original volume. Therefore, dynamic light scattering analysis conducted on the CdSe/ZnS-PAA solution yielded a nominal diameter of 41 nm with a polydispersity index of 0.28. Because DLS measures a scattered-light intensity-weighted average particle hydrodynamic diameter (Z-averageg),[50] AFM was performed to measure the sample after it was dried on a flat substrate. The quantum dots in

their dried form varied in size between 2 and 10 nm. As shown in Figure 2.8 (the green circle), AFM measures the total diameter including the CdSe core, the shell of ZnS and the thickness of the polymer. AFM yielded a nominal diameter of 8 nm with a standard deviation of 5 nm, which lies between the value of DLS and TEM. TEM measures the electrons transmitted through the specimen which affected by the electron density of each atom, so polymer coating cannot be viewed due to the lack of scattering contrast (Figure 2.8 the red circle). The optical properties of a semiconductor are critically controlled by its band gap between conduction band and valence band which related to the size of the quantum dot cores. Based on this unique property, we need to know the real size of the core, so the sample of CdSe-PAA solution without the shell of ZnS was also studied by TEM. The distributions of particle diameters are approximately Gaussian. Furthermore, TEM yielded a nominal diameter of 2.4 nm, which revealed the size of CdSe cores and CdSe/ZnS.

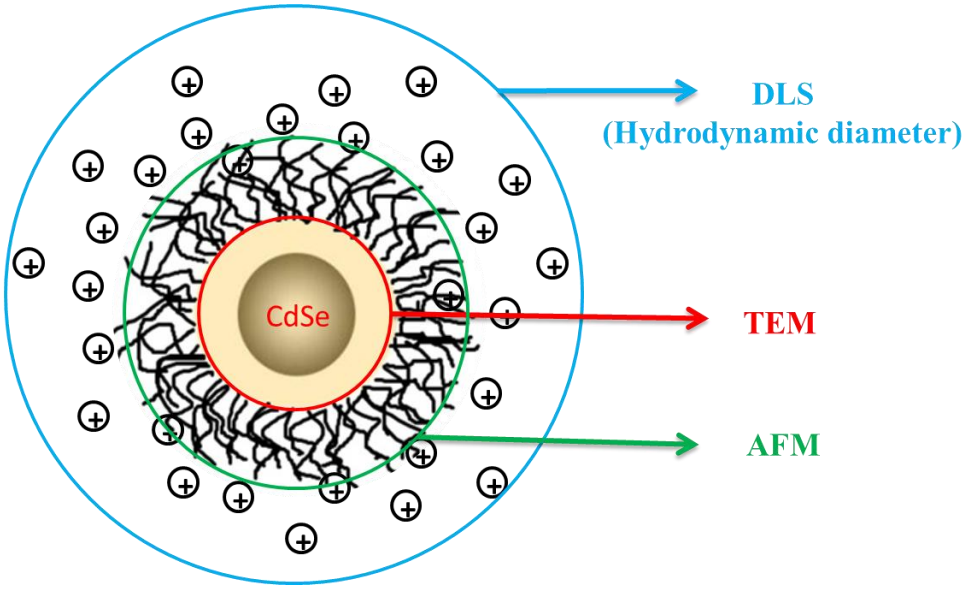


Figure 2.8 The different diameters measured by three different techniques. The blue circle shows the hydrodynamic diameter measured by DLS, the green circle shows the total diameter measured by AFM and the red circle shows the diameter measured by TEM.

In short, TEM is useful for giving a measurement of the core which measures the electrons transmitted through the specimen. AFM gives the size of the quantum dots in their dried form by measuring the forces between the tip and sample, while the hydrodynamic diameter of quantum dots measured in solution can be estimated easily using DLS.

# 3 Optical properties of the CdSe/ZnS QDs

## 3.1 Overview

In this chapter, the optical (spectroscopic) properties of the white CdSe QDs are described. The absorption and emission spectra of the QD solutions were measured using conventional steady-state optical spectroscopy. By using these characterization tools, the size and photoluminescence quantum yield of QDs were determined. In order to identify contributions from individual CdSe QDs to these ensemble average measurements, the fluorescence of samples were also measured using dual-view single-molecule fluorescence microscopy. The properties of the white QDs were compared with standard commercial QDs, using all of the same methods of analysis. The results gathered from the three different kinds of measurements are presented and discussed in this chapter.

## 3.2 Materials and methods

### 3.2.1 Materials

The samples (white QDs solution and CdSe-PAA solution) were provided by Dr.Jane Goh from University of Toronto. The Lumidot CdSe/ZnS (core-shell type commercial QDs, 532 nm) in toluene and Rhodamine 6G (R6G) were purchased from Sigma-Aldrich. The calibration spheres for single molecule fluorescence microscopy (FluoSpheres amine-modified microspheres, 0.2 μm, yellow-green) were obtained from Molecular Probes, Inc. The microscope coverglass (22 mm x 22 mm) was obtained from VWR.

### 3.2.2 Sample Preparation

Before each measurement, the white QD solution was diluted in ultrapure Millipore water to an appropriate concentration and filtered with a 0.2 μm syringe filter. The solution was then

sonicated for 10 minutes to break up any possible aggregates. The commercial QD solution was diluted in toluene to an appropriate concentration. R6G was dissolved in ethanol and calibration spheres were dissolved in ultrapure Millipore water. The thin films for emission spectra were prepared by adding 50 μL of white QD solution or commercial QD solution on glass coverslips and evaporating under ambient condition for 30-40 minutes depending on the density of particles required. Any residual solution was dried with a stream of nitrogen. For single molecule measurements, 100 μL of solution was deposited onto microscope coverglass by spin-casting (1000 rpm for 1 min). The coverglass was thoroughly cleaned using methanol and treated in a Harrick benchtop plasma cleaner under "High" for about 30 minutes to ensure a clean surface. Control samples of coverglass cleaned in this way showed no fluorescent impurities when imaged under conditions typically used for single molecule measurements. These general methods were followed for all samples.

### 3.2.3 Instrumentation

**Ensemble absorption and fluorescence measurements**

All the measurements were performed in ambient conditions with aerated solutions. Absorption spectra were recorded with a Varian Cary 500 Scan UV-Vis-NIR spectrophotometer and fluorescence emission spectra were recorded with a PTI Quantamaster spectrofluorometer. All the ensemble measurements were carried out in 10 mm x 10 mm quartz cuvettes. For fluorescence measurements, the solutions were excited at 410 nm and emission spectra were collected in the 430 – 750 nm range. Absorption spectra were collected in the 350 – 700 nm range.

**Single molecule microscope setup**

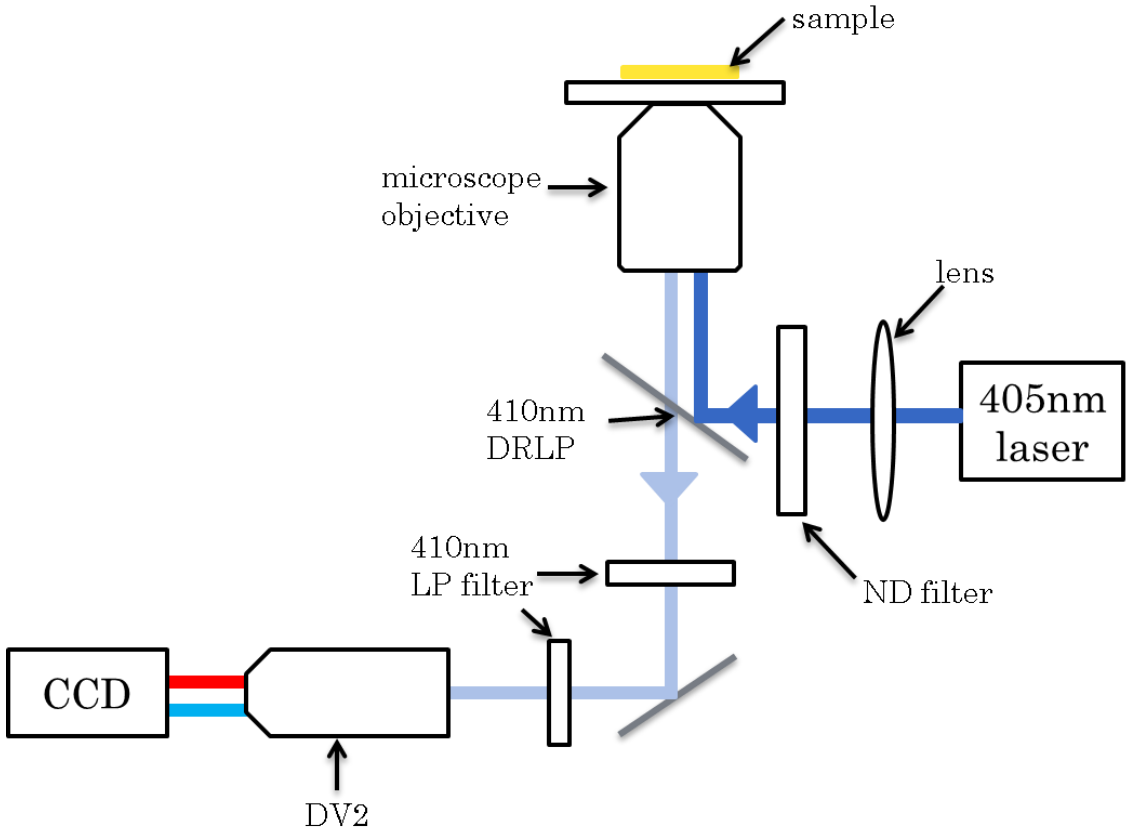


Figure 3.1 A schematic diagram of the home-built single-molecule fluorescence microscope used in these experiments. The 405nm laser is used for illumination of a sample of CdSe QDs. The emission from these is imaged onto a CCD camera through a beam splitter (DV2) which is used to separate the blue fluorescence (455 nm to 485 nm) and the red fluorescence (535 nm to 565 nm). The schematic of the commercial beam light splitter (DV2) is shown in Figure 3.2.

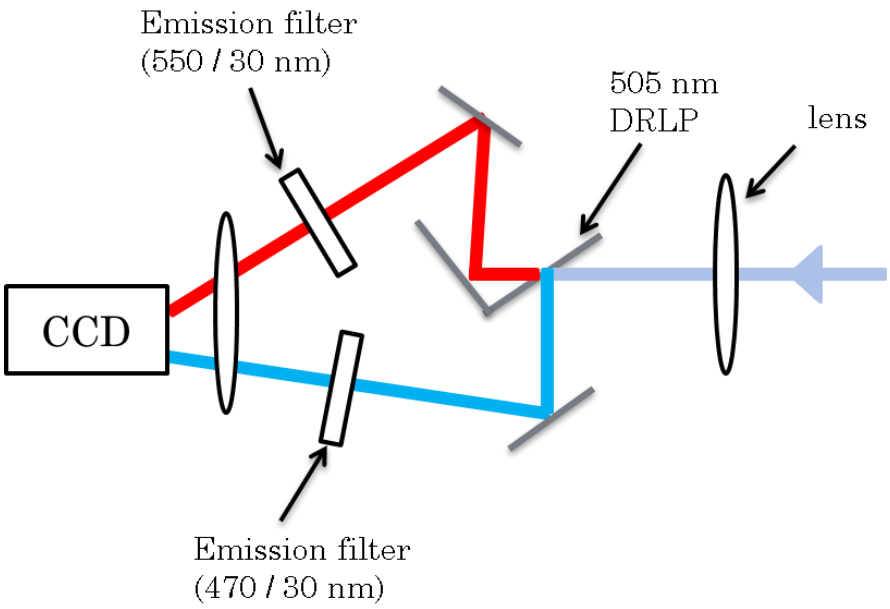


Figure 3.2 Schematic illustration of the emission path of a commercial beam splitter (DV2). The fluorescence emission from the sample can be separated by a DV2 filter cube which consists of a dichroic filter and a pair of emission filters. The separated light is adjusted by a group of mirrors and passes through an imaging lens to the CCD photodetector.

Figure 3.1 shows a schematic diagram of the home-built single molecule microscope used in these experiments. The lens focuses the excitation light onto the back focal plane of the microscope objective lens. The resulting fluorescence is collected back through the objective lens, passes through the dichroic and emission filters and is finally directed onto the CCD photodetector.

Briefly, the samples of CdSe QDs were excited by a 405 nm diode laser (Dragon Lasers). The beam was passed through a neutral density filter to attenuate laser power to 0.5 mW (measured at the microscope objective lens), and focused with a 500 mm focal length lens (Thorlabs Inc) onto the back focal plane of a 60X, 1.4NA oil-immersion objective lens (PlanApo, Nikon). Excitation light was reflected onto the sample by a 410 nm long-pass dichroic filter (a

DRLP 410 nm, Omega Optical). After excitation, the emission fluorescence from the sample was filtered through two 410 nm long-pass filters and one 405 nm notch filter (Omega Optical) to remove residual excitation light. Fluorescence collected from the sample also passes through a commercial beam light splitter (DV2) to separate the blue fluorescence (455 nm to 485 nm) and the red fluorescence (535 nm to 565 nm). The schematic of the emission path of DV2 is shown in Figure 3.2. The separated light is adjusted by a group of mirrors and passes through an imaging lens. The split image was directed to the CCD photodetector (Cascade 512F, Photometrics). CCD pixels were binned to ensure maximum possible signal-to-noise ratio in the collected emission images. Operation of the CCD photodetector and data analysis was carried out through MetaMorph imaging software, which allows for both static and time-resolved imaging. The single molecule measurements were done at 0.2 $kW/cm^2$ illumination intensity and the data were collected with 300 ms exposure time. The CCD pixels were binned to 2 in order to increase the signal-to-noise ratio.

For the characterization of the collected emission images, yellow-green fluorescent polymer spheres (505 nm absorbance / 515 nm emission) were used to determine which side was the red channel and blue channel. Figure 3.3 displays the image collected from the CCD camera and the emission spectrum of the calibration spheres. Based on the emission spectrum, the integrated intensity in the range between 455 nm to 485 nm is zero. In the other words, there is no emission fluorescence expected in the blue channel which corresponds to the left side of the image. Based on this, it can be determined that the left and right side of the image corresponds to the blue channel and the red channel, respectively.

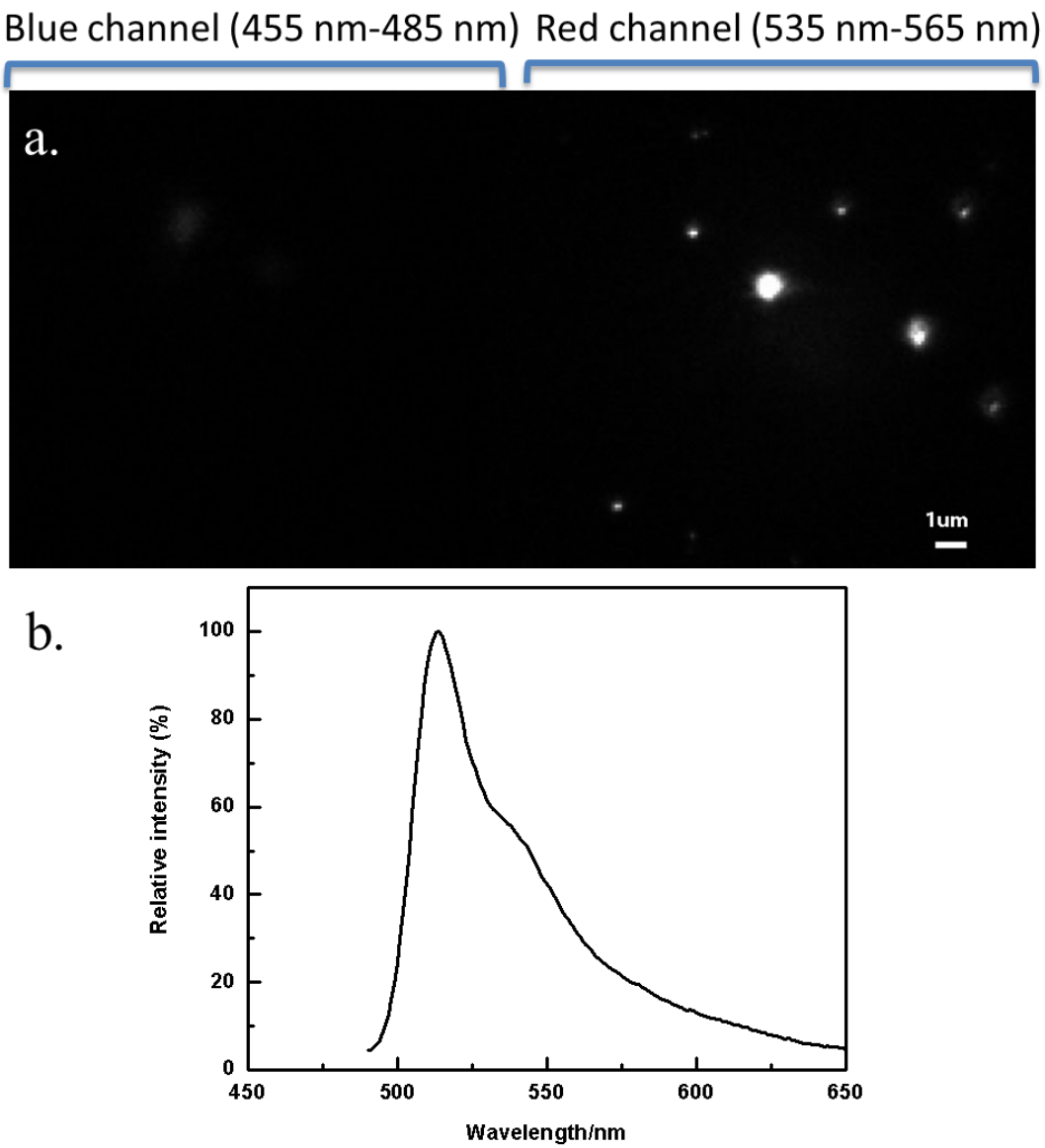


Figure 3.3 (a) The single particle fluorescence image of yellow-green fluorescent polymer spheres (505 nm absorbance / 515 nm emission). There is no fluorescence in the left side of the image. (b) The emission spectrum of yellow-green fluorescent polymer spheres. The integrated intensity in the range between 455 nm to 485 nm is zero.

The two image channels are slightly offset from each other, and it is important to be able to exactly determine the same position in each channel. To locate the same quantum dot in both

channels, fluorescent polymer spheres which have a broad emission spectrum were used. Figure 3.4 indicates the fluorescence signal can be viewed in both channels. The labelled areas indicate the two corresponding spots originated from an identical spot on the sample slide. The position of each individual spot in both channels was labelled in an area of 4 x 4 pixels (400 nm x 400 nm). Based on 127 pairs of corresponding spots, we determined that the corresponding positions were offset by 171 pixels in the X-axis and by 16 pixels in the Y-axis.

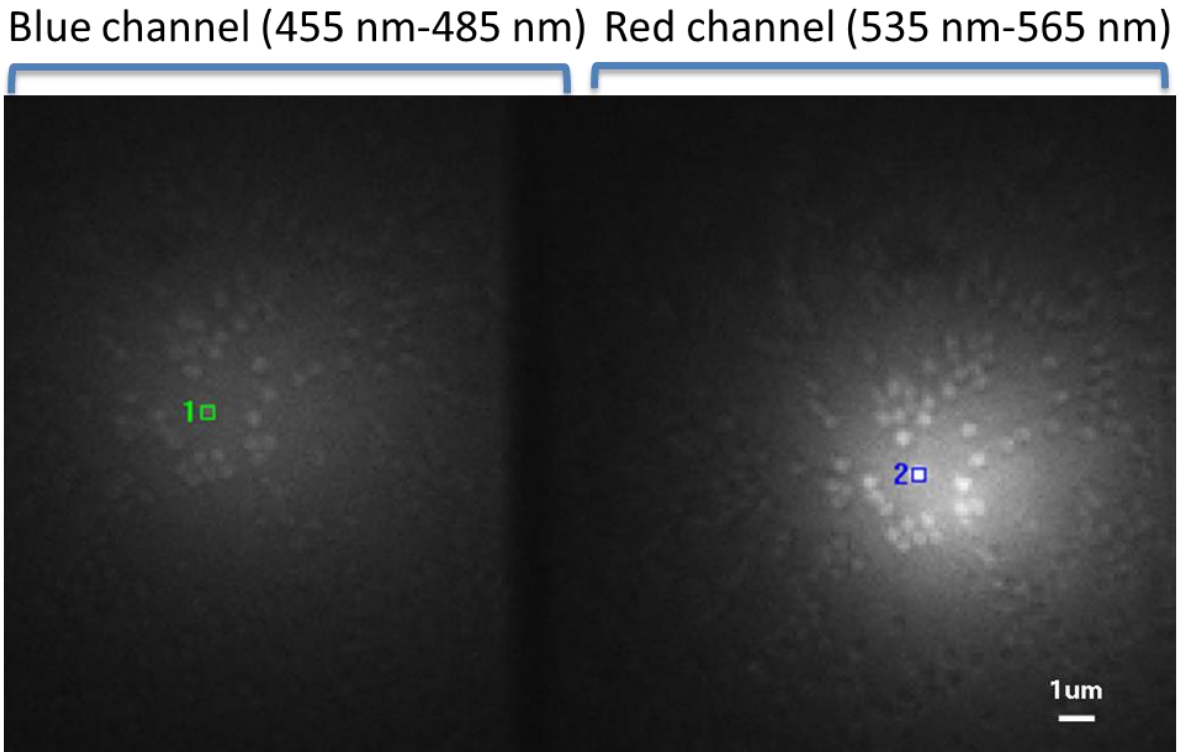


Figure 3.4 The fluorescence image of white fluorescent polymer spheres. The fluorescence signal can be viewed in both channels. The labelled areas indicate the two corresponding spots originated from an identical spot on the sample slide.

## 3.3 Results and discussion

Figure 3.5 shows an optical photograph of the white QD solution in water under ambient and UV light (254 nm) illumination. The solution is yellow under ambient conditions, while it yields a white emission under UV-visible light illumination which displays the wide spectral range of luminescence.

Figure 3.5 Photograph of nanoparticle solutions under ambient and UV visible light illumination provided by Dr. Jane Goh.

### 3.3.1 Absorption spectra

Figure 3.6 shows the UV absorption spectra for the commercial QDs in toluene and the white QDs in water. The spectrum and the absorption peak of the commercial quantum dots were in good agreement with data provided by the manufacturer. Compared with the commercial quantum dots with a sharp absorption edge at 510 nm, a broad edge centered at about 440 nm

can be found in the absorption spectrum of the white quantum QDs. The broadening of the spectrum can be attributed to a number of factors, such as the shapes of QD, the size distributions and surface defect states.[51] As mentioned previously, the absorption and emission feature are highly dependent on the size of nanoparticle. Small changes in the size will cause differences in optical features. The size of commercial QDs is around 3.3 nm according to manufacturer. The band gap of a semiconductor is defined as the energy difference between the highest level of the valance band and the lowest level of the conduction band.[52] Due to the effect of quantum confinement, the band gap gets larger with reducing the core diameter of nanoparticles. Therefore, the absorption spectrum of the white quantum dots should be blue-shifted to a shorter wavelength based on the average core size of 2.4 nm determined from the TEM measurements.

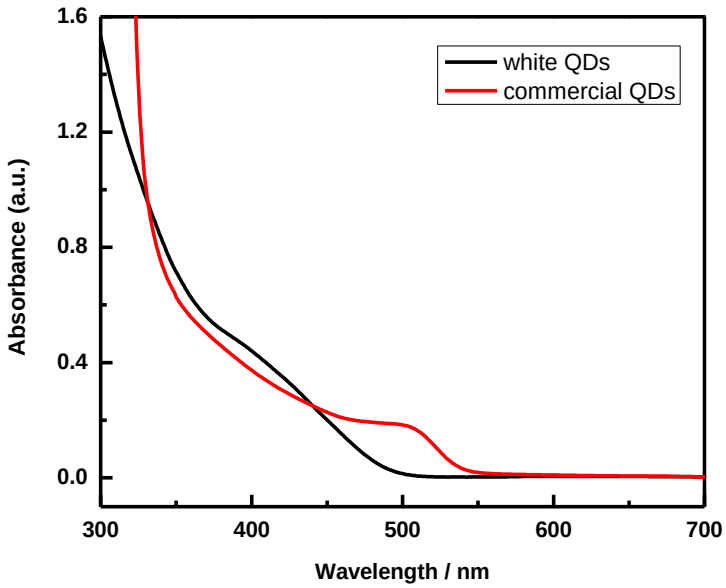


Figure 3.6 Absorption spectra of the commercial QDs and white QDs. The black line is the absorption spectrum of white QDs, while the red line is the absorption spectrum of commercial QDs.

Furthermore, the absorption spectra can also be used to obtain the mean size of the QDs based on the position of the absorption edge. Light with lower energy photons than the band gap energy cannot be absorbed, while that with higher energy photons can be absorbed. The minimum photon energy for electron transition from valance band to conduction band will correspond to the band gap energy.[52] The simplest way to estimate the band gap energy of the semiconductor is taking the wavelength when the sample starts to absorb light. To accomplish this, a straight line was fit to the absorption shoulder and the x-axis intercept was taken to be the band gap energy. Using this approach, the spectral data for the commercial QDs gave an x-axis intercept of 543 nm with an uncertainty of 9 nm, while the x-axis intercept of the white quantum dots was at 490 nm with an uncertainty of 2 nm. The observed wavelength can be converted to band gap energy by the following equation:

$$E = \frac{hc}{\lambda} \qquad (3.1)$$

where E is the band gap energy in J, *h* is Planck constant in J·s, c is the speed of light in m/s and λ is the measured wavelength in m. The calculated band gap energy of commercial QDs and white QDs were 2.28 ± 0.03 eV and 2.53 ± 0.01 eV, respectively. White QDs show a larger energy band gap than that of commercial QDs. The size-dependent band gap is one of the most important parameter of semiconductors, so there are several methods found by people to investigate this phenomenon.[3,53,54] However, it should be taken into consideration that different models might yield slightly different sizes. Baskoutas et al and his group developed a model based on the effective-mass approximation (Equation 1.1) which shows good agreement between theoretical predications and experiment data.[4] The calculation in this model can be followed by:

$$\left[\frac{p_i^2}{2m_i^*} + U_i(r_i)\right]\phi_i(r_i) = E_i\phi_i(r_i), \quad i = e, h \qquad (3.2)$$

$$E(r) = E_{gap} + (E_e + E_h) \qquad (3.3)$$

where $m_i^*$ is the effective electron (hole) mass, p is the momentum , $U_i(r_i)$ is the self-consistent effective field, $E_{gap}$ is the band gap of bulk material. The effective band gap is given by Equation 3.3. Based on their results and our calculated band gap energy, we estimated the average particle size of commercial QD is 3.2 ± 0.2 nm which agrees well with the data provided by the manufacturer. The average particle size of white QD is around 2.4 ± 0.1 nm. The size measurement by TEM indicates the commercial QD was 3.1 ± 0.5 nm and the white QD with the shell was 2.4 ± 0.3 nm, which were in good agreement with what was found from the absorption spectra.

As described in the size measurement by TEM, it could not be determined whether there was a shell of ZnS capping the core. Therefore, the absorption spectrum of CdSe-PAA sample was also analyzed under the same conditions to see whether there was any difference from CdSe/ZnS-PAA sample. Figure 3.7 shows the absorption spectra of white QDs before (red line) and after (black line) overcoating with ZnS. The measurements show the absorption edge underwent a small red-shift after overcoating, an effect that has previously been assigned to the transition of excitons into the ZnS matrix.[55,56] The high surface-to-volume ratio of small QDs results in a more evident red shift where the leakage of the excitons into the shell is more sensitive to the quantum confinement.[56] In other words, the effect of quantum confinement will decrease with the increasing of the size of QD, therefore, the absorption edge will red-shift to longer wavelengths. Based on the cut off wavelength of the CdSe-PAA sample (482 ± 3 nm), we calculated the band gap energy was 2.57 ± 0.01 eV using the same method described above,

which corresponds to an estimated average particle size of 2.2 ± 0.1 nm. This number was slightly smaller than the data found using size characterization tool TEM, 2.4 ± 0.5 nm. As noted previously, the size of CdSe-PAA showed no significant difference with the size of CdSe/ZnS-PAA. However, it was suggested from the absorption spectra that there was a thin shell of ZnS coated CdSe core whose thickness is around 0.2 nm.

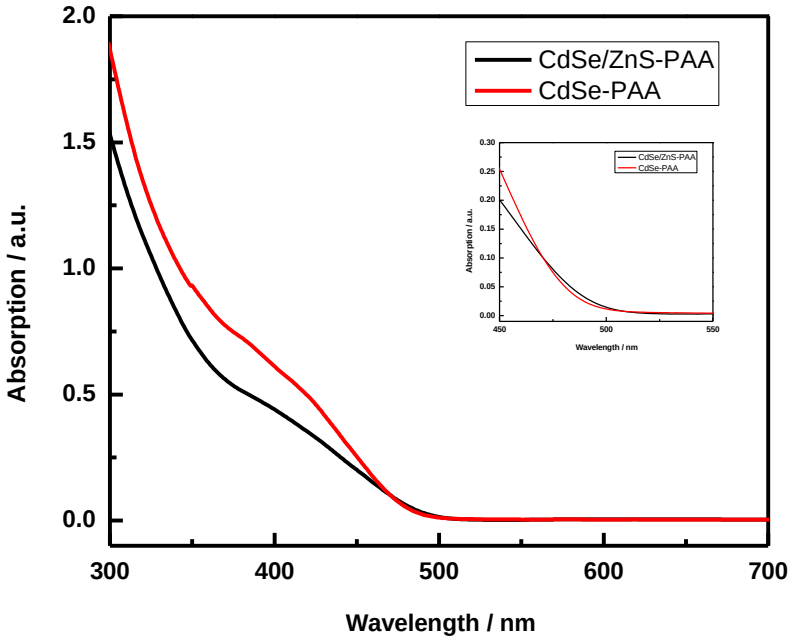


Figure 3.7 Absorption spectra of white QDs (CdSe/ZnS-PAA) and before overcoating with the shell of ZnS (CdSe-PAA). The black line is the absorption spectrum of white QDs, while the red line is the absorption spectrum of CdSe-PAA. The inset shows the band edge absorption.

### 3.3.2 Photoluminescence spectra

Quantum confinement also affects the fluorescence emission spectra. The emission feature can be tuned by adjusting the size of nanoparticles. Increasing the size of particles causes the emission peak to shift to longer wavelengths.

To compare the emission spectrum with the commercial QDs, both results are shown in Figure 3.8. The black lines show the emission spectrum of QDs dispersed in solution, while the red lines show that of QDs deposited and dried onto a glass slide. The emission data from the commercial QDs (Figure 3.8 (a)) also matched well with the published values and show a narrow photoluminescence (PL) spectrum with a pronounced peak at 530 nm. In contrast, the PL spectrum of the white QDs covered nearly the entire visible spectrum with a main peak at around 480 nm and a weaker peak at around 580 nm. We attribute the blue emission to the band gap emission which occurs by the direct recombination between the edge of conduction band and valance band. Therefore, this emission feature has a strong dependence on the size of QDs. On the other hand, the red emission peak resembles deep trap emission which occurs by the indirect recombination between an electron or a hole trapped in a state that is energetically in the middle of conduction band and valance band.[22] These trap states have been attributed to defects in their crystalline structure and missing or extra atoms which can be easily found in small QDs due to the high surface-to-volume ratio.[25] A red-shift between the spectra of the white QDs measured in solution and thin film is also readily apparent. The drying process can contribute to the red-shift of the emission spectrum due to the interaction between QDs in close proximity and between a quantum dot and substrate. This interaction leads to the aggregation of QDs followed by a decrease of quantum confinement.[57] Therefore, the band gap emission, which corresponds to the blue peak, is red shifted to a longer wavelength, while the weaker peak arising from the deep trap recombination remained at the same wavelength after it was dried on the glass. Broad emission spectrum of white QDs was observed and compared to the narrow spectrum of the commercial QDs.

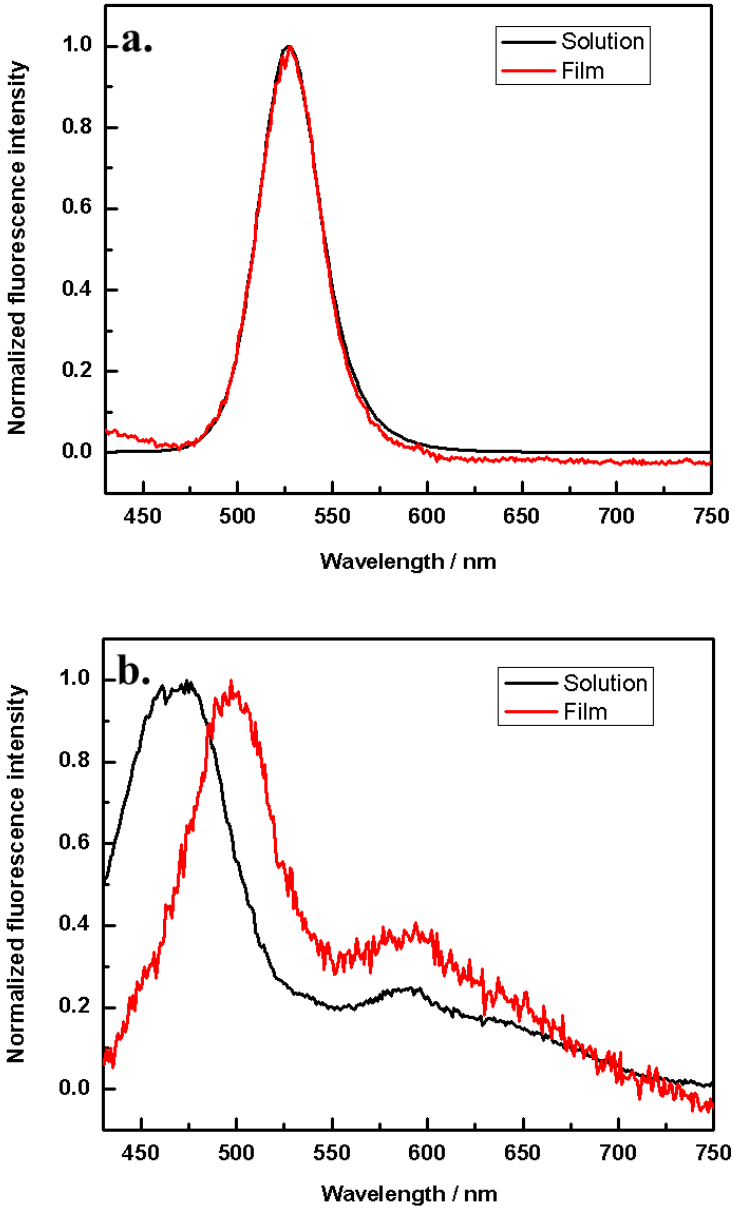


Figure 3.8 (a) Photoluminescence spectra of the commercial QDs in solution (black line) and thin film (red line) with a peak at around 530 nm. (b) Photoluminescence spectra of the white QDs in solution (black line) and thin film (red line).

In order to observe the influence of the thin shell of ZnS on the emission features, the concentration of both CdSe-PAA and CdSe/ZnS-PAA samples were adjusted to match the absorbance at the excitation wavelength. Figure 3.9 (a) shows the absorption spectra of CdSe-PAA and CdSe/ZnS-PAA and the arrow points to the matched wavelength at 410 nm which was used for excitation. Moreover, the absorption spectra almost overlap each other. Therefore, one can reasonably assume that they have the same concentration and can absorb the same number of photons. Figure 3.9 (b) shows the photoluminescence spectra of white QDs before (red line) and after (black line) overcoating with the shell of ZnS. The PL intensity was much lower in the absence of the shell, likely because of the large amount of surface defects which can cause an overall decrease in fluorescence emission. In other words, the stronger emission with ZnS shells was the result of quenched surface states by the shell. Moreover, this has been achieved owing to the wider band gap of ZnS (Figure 3.10). As a higher band gap material, ZnS not only passivates the surface bonds and prevent the photooxidation but also supply a better confinement of photogenerated electrons and holes inside the core of CdSe.[25,58] To determine the influence of the shell on the position of peaks, the PL spectra were normalized (Figure 3.9(c)). In contrast to the PL spectrum of the capped particles, the red emission was stronger than the blue emission arising from the band gap emission. The strong red emission could be attributed to the recombination of photons trapped in the deep trap states which lies between the edge of conduction band and valance band resulting in a lower energy emission. It is worthwhile noticing that the number of trap states arising from the surface increases with a reduction of the diameter of QDs.[21,26,59] Due to the high surface-to-volume ratio, the broad emission spectrum of CdSe-PAA was dominated by the deep trap emission from the surface defects with a weak band gap emission. Overcoating with the shell of ZnS prevents the lower energy emission by passivating

the non-radiative sites from the crystalline surface, resulting in an enhanced band gap emission and a quenched deep trap emission. After overcoating, the PL spectrum is dominated by a stronger blue band edge emission and a weaker red emission.

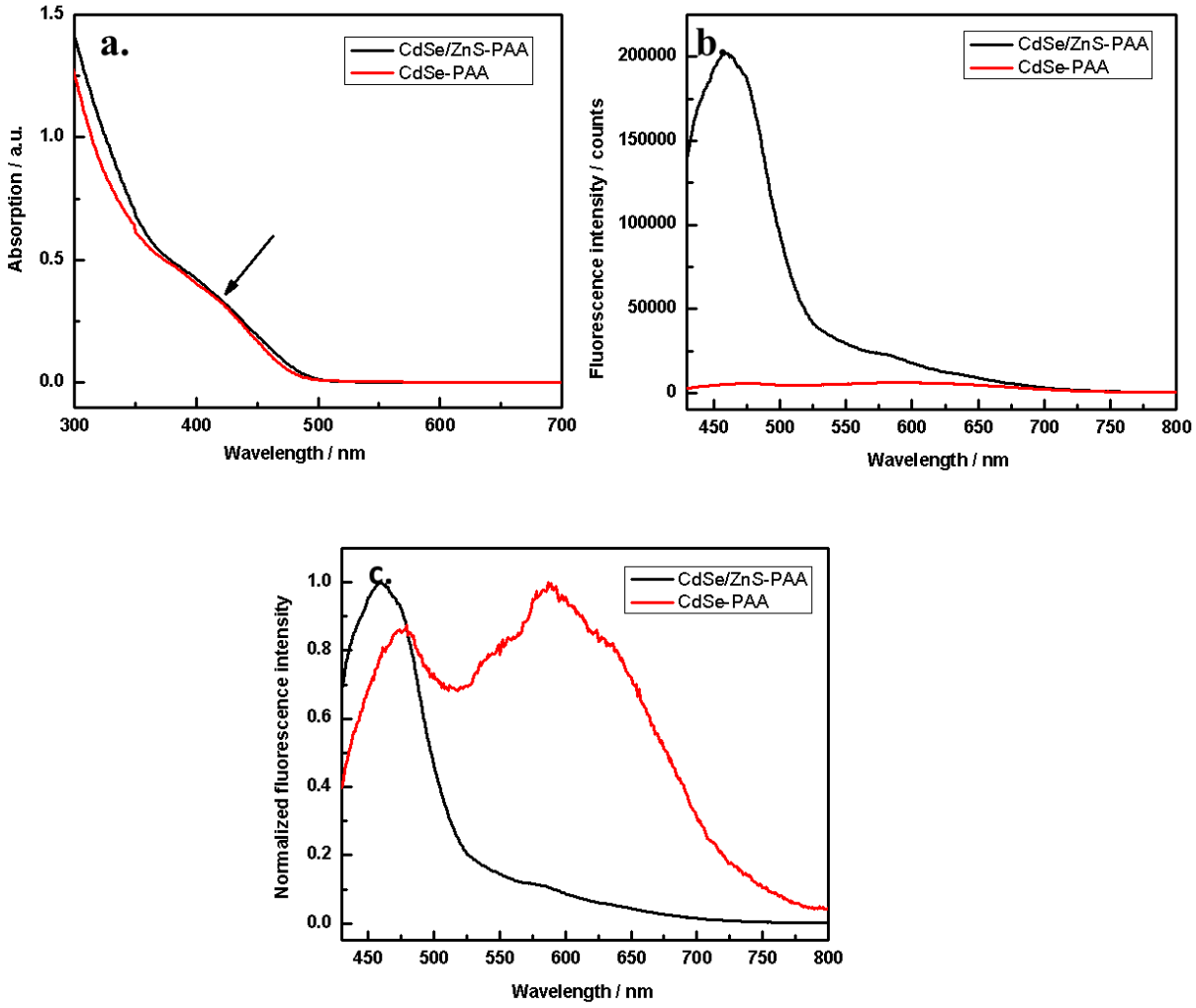


Figure 3.9 (a) Absorption spectra of the CdSe/ZnS-PAA sample (black line) and the CdSe-PAA sample (red line). (b) Photoluminescence spectra of the CdSe/ZnS-PAA (black line) and CdSe-PAA (red line) with a same excitation wavelength at 410 nm. (c) Normalized photoluminescence spectra of those two solutions.

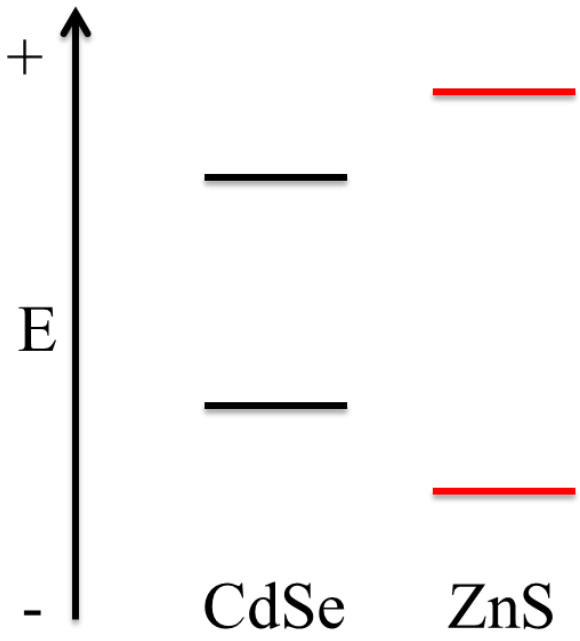


Figure 3.10 Band gap diagram of CdSe and ZnS.

### 3.3.3 Quantum yield

Fluorescence quantum yield is defined as the ratio of the number of fluorescence photons emitted by a molecule to the number of photons absorbed. The easiest way to estimate the quantum yield of a fluorophore is by comparison with standards of high known quantum yield. According to their absorption and emission spectra, we need to choose a reference dye that emits in a similar region of the spectrum for reliable comparison. For the measurements described here, Rhodamine 6G (R6G) which emits in the visible region and exhibits a known quantum yield of 94% in ethanol was selected as the reference.[60] Moreover, to calculate the quantum yield using this approach, the absorption and emission spectra of both the standard sample and test sample are needed. The estimated quantum yield of CdSe/ZnS-PAA was compared to that of commercial QDs and CdSe-PAA. Figure 3.11 displays the absorption and emission spectra of R6G, CdSe/ZnS-PAA, CdSe-PAA and commercial QDs.

As shown in the absorption spectra (Figure 3.11 (a)), the arrow points to the matched wavelength where the optical density of R6G was equal to that of commercial QDs. Both of the sample and reference have the same absorbance (never exceed 0.1 to minimize any re-absorption) at the same excitation wavelength. Therefore, 500 nm was chosen for excitation of R6G and commercial QDs. The emission spectra measurements were performed under the same instrumental condition and recorded in the range from 510 nm to 800 nm for calculating the integrated fluorescence intensity in that area. Finally, the quantum yield was calculated using the following equation:

$$Q = Q_R \frac{I}{I_R} \frac{OD_R}{OD} \frac{n^2}{n_R^2} \qquad (3.3)$$

where Q is the quantum yield, I is the integrated intensity, OD is the optical density and n is the refractive index of the solvent. R refers to reference which was R6G. The calculated quantum yield of commercial QDs was 42% which agreed with the value provided by the manufacturer. For the white QD samples, the emission spectra were measured at an excitation wavelength of 450 nm where both the QDs and the R6G solution had the same absorbance. The integrated fluorescence intensity was calculated under the area of the emission spectra curve. In comparison to the commercial QD, the estimated quantum yield of CdSe/ZnS-PAA is much lower with a value of 5% using the same method. The sample of CdSe-PAA had the lowest quantum yield of less than 1%, which was in good agreement with what we observed in the fluorescence emission spectra. The addition of a ZnS shell enhanced the quantum yield as well by quenching the surface defects.

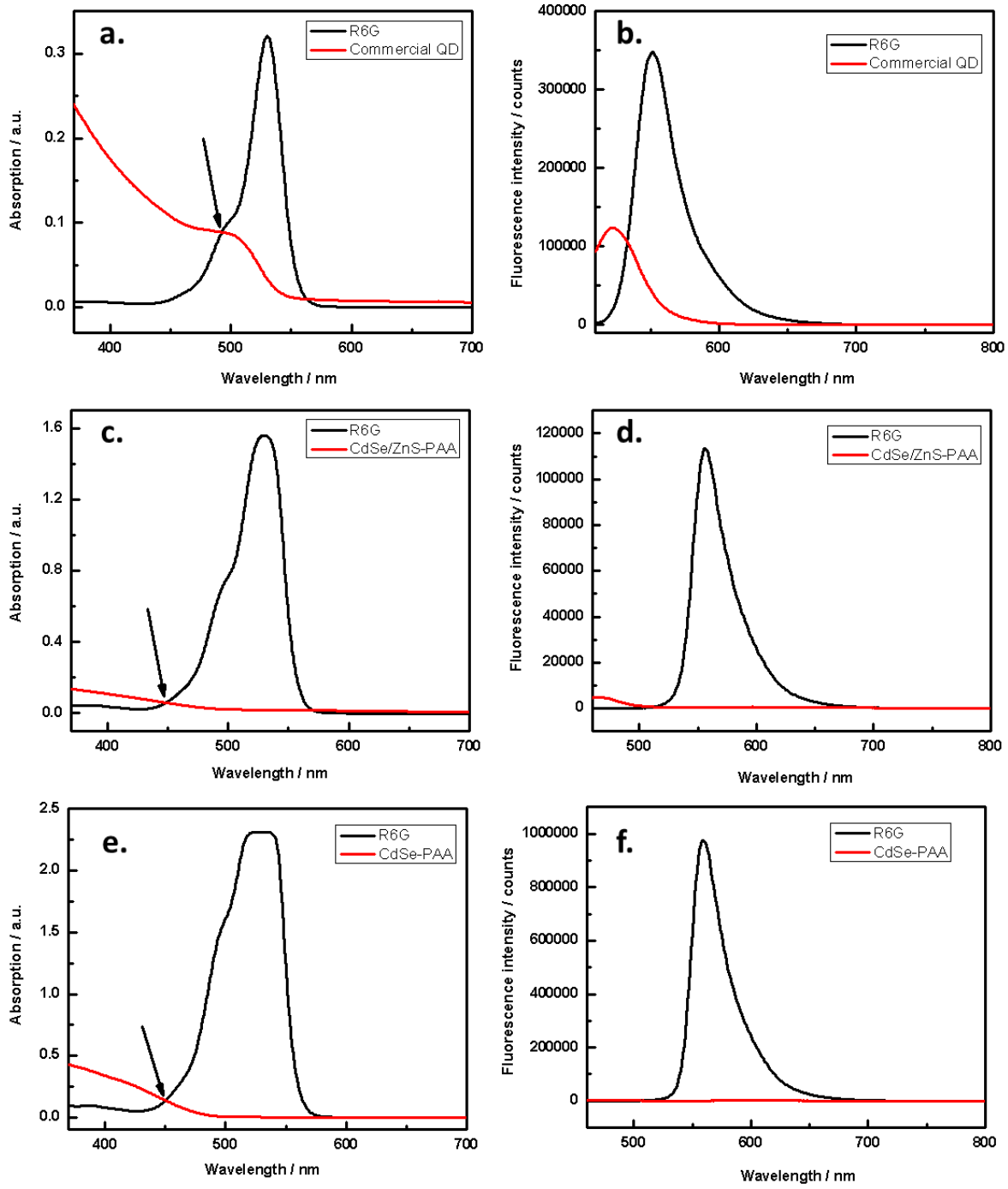


Figure 3.11 (a)(b) The absorption and emission spectra of R6G and commercial QDs. (c)(d) The absorption and emission spectra of R6G and CdSe/ZnS-PAA. (e)(f) The absorption and emission spectra of R6G and CdSe-PAA. The arrows point to the matched wavelength which was used for excitation.

### 3.3.4 Dual-view single molecule fluorescence microscopy

To explore the behavior of each single QD, single-molecule fluorescence measurements were carried out using a home-built microscope. The dual-view SM fluorescence microscope is described in the Materials and Methods section (3.2.3).

Typical fluorescence images of commercial QDs and white QDs are shown in Figure 3.12. Single quantum dots were distinguished from the background and aggregates by locating spots which displayed ON and OFF states (photoblinking) under continuous illumination. The numbered, labelled areas in Figure 3.12 indicate the two regions that come from an identical single QD on the sample slide, and the arrow points at an aggregate that did not exhibit photoblinking. In the images of commercial QDs, there were no aggregates detected. However, aggregates in the white QD samples were occasionally observed. This agrees with the ensemble PL spectrum measured for thin film which indicates the samples tend to aggregate on the glass.

No fluorescence signal was observed in the blue channel for commercial QDs and no fluorescence signal was observed in the red channel for the white QDs. Compared with the fluorescence image of commercial QDs, there is no red emitting QD in the CdSe/ZnS-PAA sample since we could not find any fluorescence signal of an individual spot in the red channel. According to this point, the white QDs did not consist of a mixture of different color emission QDs, but rather each dot emitted “white” light, similar to what is shown in Figure 3.8b.

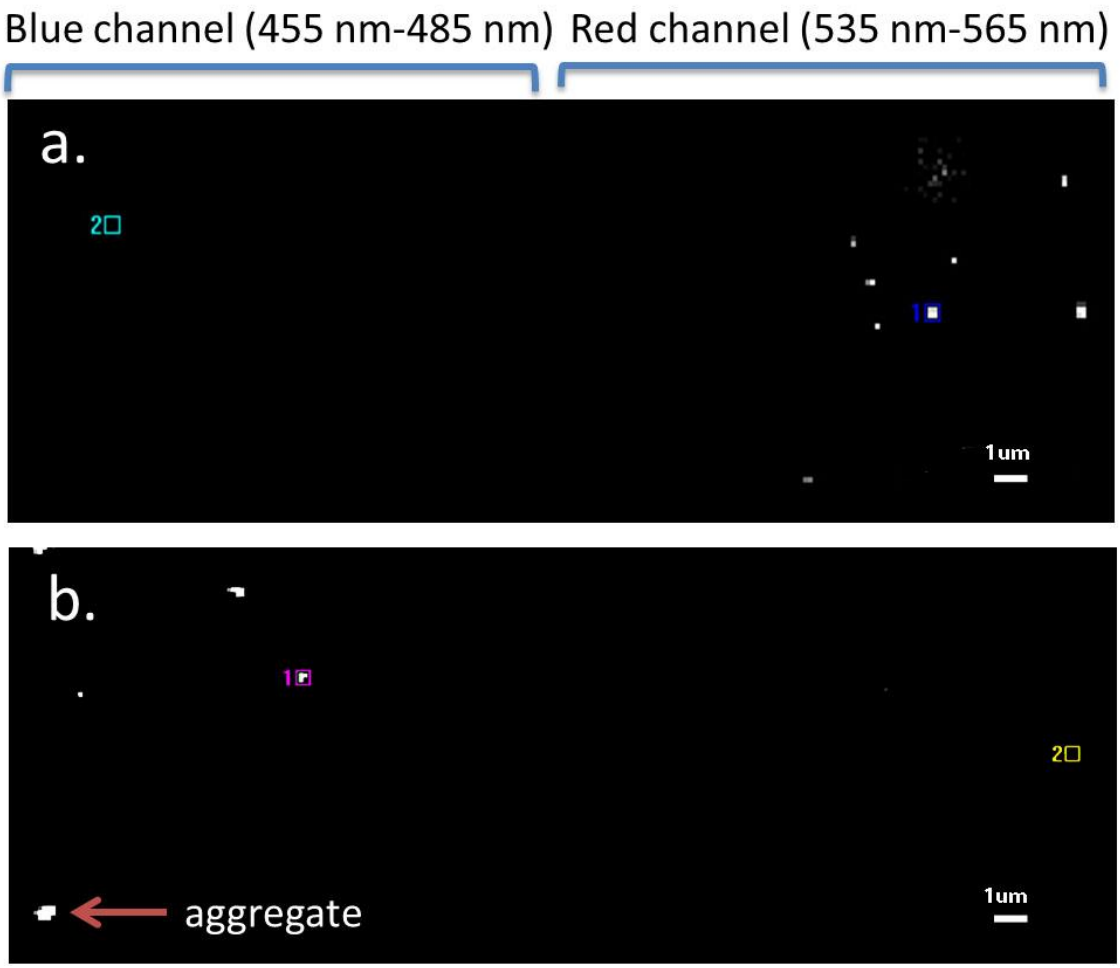


Figure 3.12 Fluorescence images of commercial QDs (a) and white QDs (b). The left and right sides of image corresponds to the blue and red channels, respectively. The labelled areas with number indicate the two corresponding single molecule spots in an area of 4 x 4 pixels (400 nm x 400 nm) that originated from an identical single quantum dot on the sample slide. (Excitation intensity = 0.2 kW/cm$^2$)

A simple and useful approach to data analysis in SM fluorescence experiments is to generate plots of fluorescence intensity of an individual molecule as a function of illumination time (a fluorescence time trajectory). Those plots can be made by measuring the fluorescence emission intensity from a spot over a series of sequential images, and can provide fundamental insight into the basic photophysical behavior of the fluorophore. For example, the photoblinking

of a single QD can be observed by measuring the fluctuation of the intensity against time. Moreover, it can be used to distinguish aggregates from individual QDs.

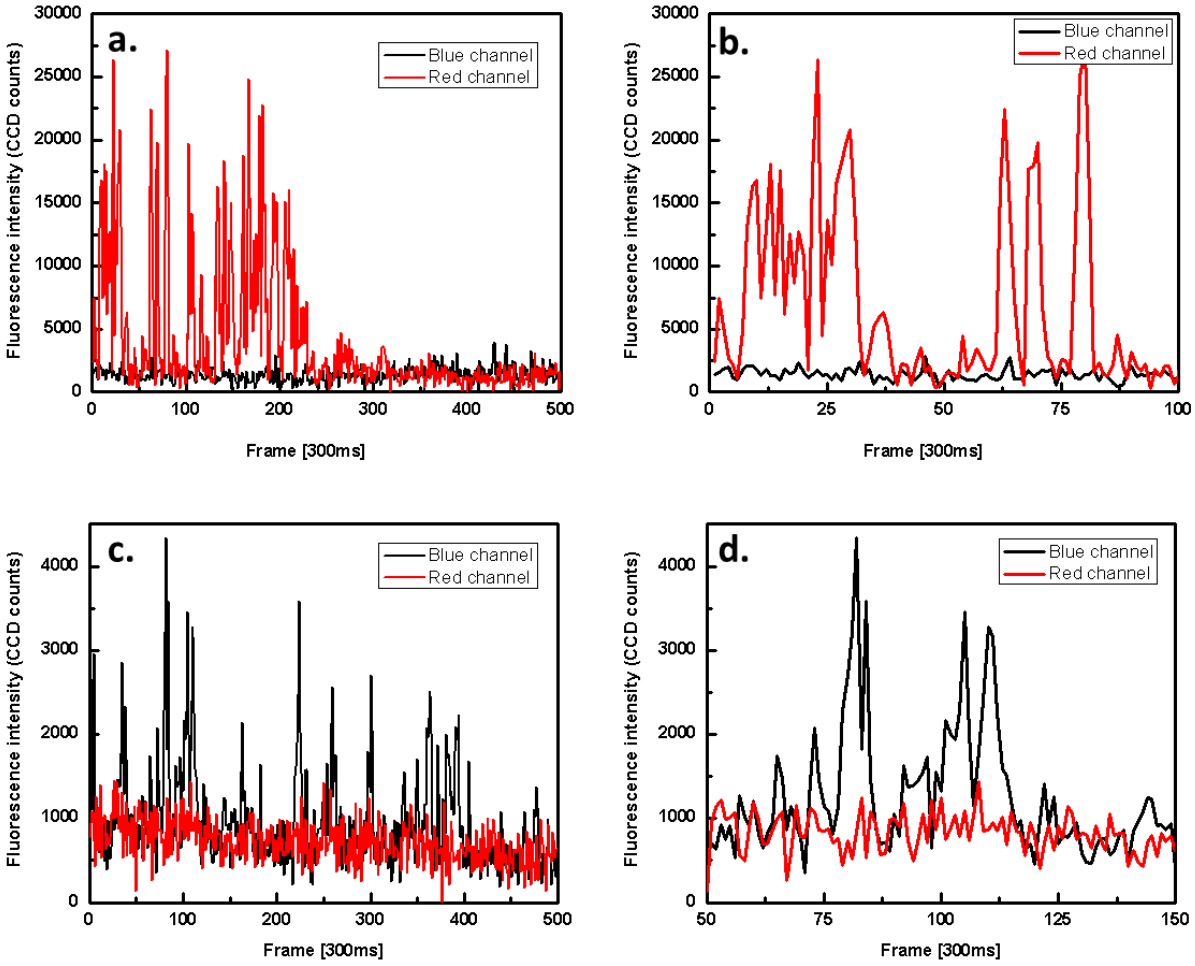


Figure 3.13 Typical single-molecule fluorescence time trajectories of a commercial QD (a) (b) and white QD (c) (d), respectively. Measurements were done at 0.2 kW/cm$^2$ illumination intensity. (b) (d) show 100 frames of the total 500 frames in (a) (c).

A typical fluorescence time trajectory, corrected for background, is presented in Figure 3.13 (a) (c). Note, this is still a two-colour experiment, in which both the blue and red emission can be monitored simultaneously. The background image used for correction purposes was taken in a

region close to the QDs. The intensity of each individual QD in each frame of both channels was measured in an area of 4 x 4 pixels (400 nm x 400 nm), as shown in Figure 3.12. The traces show repeated appearance and disappearance of fluorescence emission which is referred to as photoblinking. There has been interest in investigating the mechanism of QD photoblinking in recent years. Two main mechanisms for QD blinking have been proposed, but the mechanism of this phenomenon is still unclear so far.[61-63] A commonly believed mechanism is known as Auger ionization. In the excitation process, an electron will be excited into the conduction band leaving a hole in the valance band. Multiple photons can be absorbed with multiple photoexcited electron-and-hole pairs resulting in an ejection of either an electron or a hole to form a charged QD owing to their strong interaction energy. At this point, if a new exciton formed, it will decay through fast, non-radiative recombination instead of radiative fluorescence because this non-radiative recombination occurs much faster, which forms the first type of off-state. After this process, the QD returns to the normal fluorescence cycling.[64,65] The other theory has been proposed to have a "hot" photoexcited electron trapped in the trap states on the QD surface, where the off state is not associated with a decreased fluorescence lifetime. Instead of relaxing back to the ground state, the electron goes to the trap state on the surface of the QD and returns to the ground state through non-radiative pathways.[62,63] This kind of photoblinking can be suppressed by applying an external potential. In this case, the trap states will be occupied by the external electrons instead of the electrons from the core of quantum dots. One can control the second blinking mechanism by adding a wider band gap shell, such as ZnS or CdS, to passivate potential trap states on the surface. In both cases, nanocrystals tend to switch between on and off states more often ("flickering") resulting in an increase off states occurrences at higher intensity. According to Li's work, QDs that contain a large number of surface trap states undergo

flickering instead of blinking at high illumination intensities.[7] As shown in the single-molecule fluorescence time trajectories for the commercial QDs and white QDs, both of them flicker with unclear on and off states, especially the white QDs. The phenomena are more clearly reflected in Figure 3.13 (b) (d), which shows only 100 frames of the total 500 frames in (a) (c).

Frequency spectra (histograms) of fluorescence intensity for both types of QDs were measured over 500 frames and were fitted with two Gaussian peaks as shown in Figure 3.14 (a) (b). The binning size of histograms and the position of two Gaussian peaks were obtained by Origin. Both sets of QDs showed a relatively clear off-states and a long tail in the on-state histogram due to significant intensity fluctuations. This is the best method to analyze the on-state as the ratio between the on-state peak area and the total area under the curve, but in this case, it is difficult to find a clearly defined on-state. As is shown in time trajectory Figure 3.13 (b) (d), the single QD kept flickering with no clear on-states and off-states. The signal-to-noise ratio (SNR; defined as the mean signal corrected for background divided by the standard deviation of the signal) of the commercial QDs was higher than that of white QDs, which also had a broad distribution of on-state intensity values. Qualitatively, we observed here that the mean fluorescence intensity of commercial QDs is much higher than that of white QDs. This could be attributed to the different capping materials. The commercial QDs were capped with ZnS and further modified with hexadecylamine (HDA) which is a common stabilizer in nanoparticle synthesis. HDA plays a significant role in the enhancement of the fluorescence emission by passivating the surface defects for QDs.[66] As described in the synthesis process of white quantum dots, all the white QDs were grown in a nanotemplate made of PAA. PAA, as a polymer, has a longer molecule chain than the HDA chain which results in a thicker layer of capping materials. The size measurement by AFM reveals there was a thick layer of PAA

compared to the result obtained by TEM. The lower fluorescence intensity of white QDs is the result of several trap states on the surface.

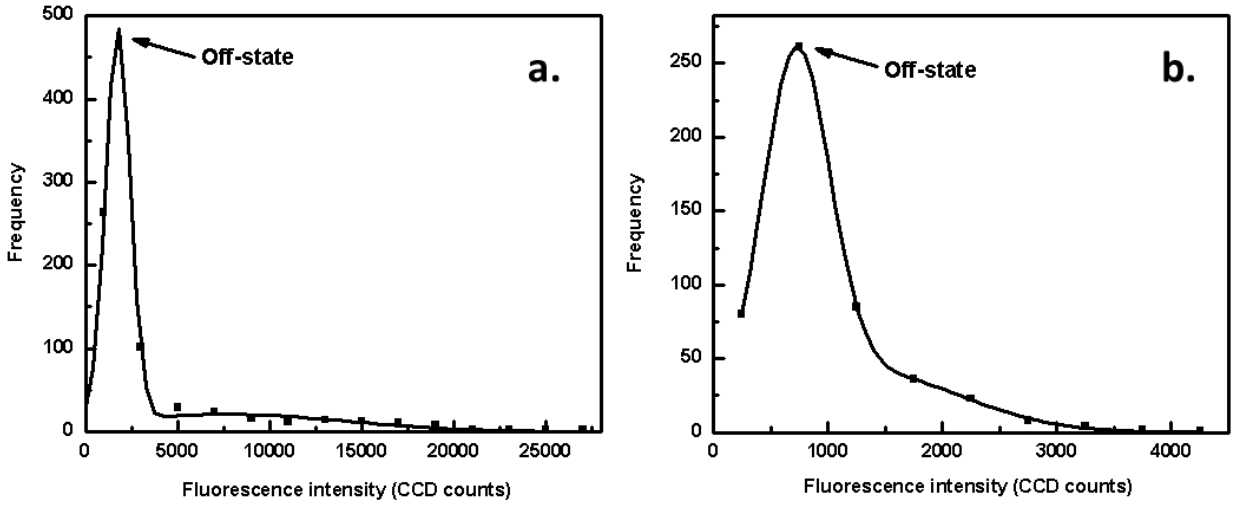


Figure 3.14 Fluorescence intensity histogram fitted with two Gaussian peaks, (a) commercial QDs and (b) white QDs, indicating the on-state and off-state separately.

To quantitively calculate the average intensity of the on-states, a threshold separating on states from off states was set at two and a half times the standard deviation of the average background counts by assuming that the distribution of background counts follows the Gaussian distribution. Under these conditions, one is 98% sure that the values which were larger than the threshold were from on-states. These values were used to find the average intensities. Based on this method, 212 commercial QDs and 329 white QDs (424 and 658 corresponding spots) were measured from each sample slide. As shown in Figure 3.15 (a), (c), 182 (86%) of commercial QDs and 274 (83%) of white QDs measured were individual quantum dots and the remaining objects were aggregates. If the quantum dots did not exhibit fluorescence intermittency or the intensity decreased systematically as a function of time, they were considered to be aggregates.

Figure 3.15 (b) (d) show two histograms of single-molecule intensities (in CCD counts, taken under the same illumination and image collection conditions) measured for commercial QDs and white QDs, respectively. The distributions show approximately Gaussian distributions. From the distribution, the average intensity of commercial QDs (10487 ± 4032 CCD counts) is much higher than that of white QDs (1083±274 CCD counts). This observation is in good agreement with the quantum yield (commercial QDs of 42% and CdSe/ZnS-PAA of 5%). For each individual QD, the intensity of commercial QD was approximately ten times of that of white QD. In other words, as they absorbed nearly the same quantity of photons, the number of photons emitted by commercial QDs was ten times of that of white QDs. Based on the ensemble PL spectra of two kinds of QDs deposited on the glass, the integrated intensity was calculated for each range. The calculated intensity ratio between blue channel and red channel of commercial QDs was 1:17, while that of white QDs was 2:1. Therefore, for commercial QDs, the intensity in the blue channel was expected to be around 600 CCD counts, while the intensity of white QD in red channel was expected to be around 500 CCD counts. This indicates that the integrated intensity of commercial QDs in blue channel and that of white QDs in red channel was too low to be distinguished from the background (shown in Figure 3.12). That is why we could not observe any fluorescence signal in blue channel for commercial QD and red channel for white QD.

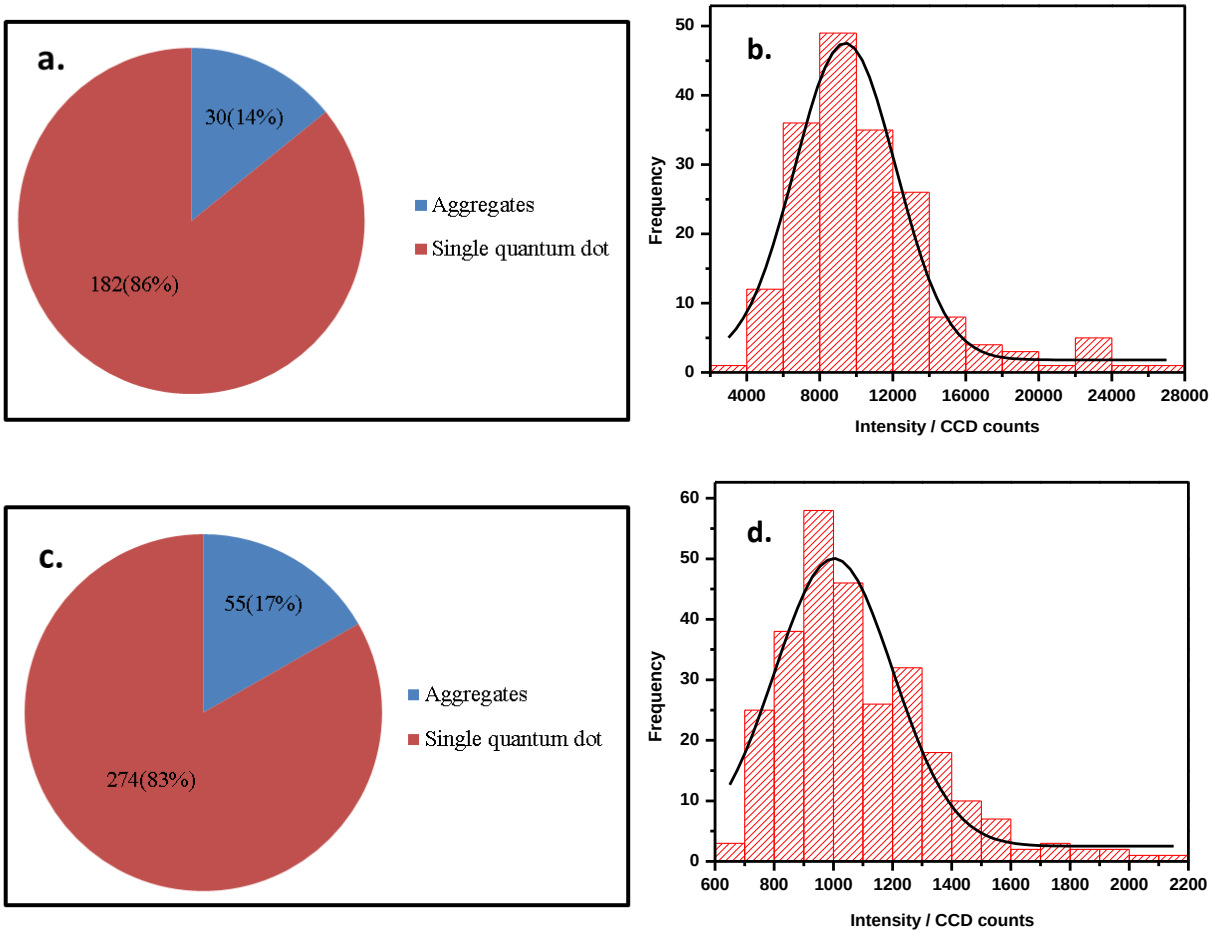


Figure 3.15 (a) (c) Pie charts showing distributions of the different types particles for commercial QD and white QD samples, respectively. (b) (d) Histograms of single-molecule fluorescence intensities for commercial and white QDs. The distributions show an approximately Gaussian distribution. In both cases, the excitation intensity was 0.2 kW/cm$^2$.

It is worth noting that there was a distribution of fluorescence intensities for a particular sample at the same experimental condition. This can be attributed to several different effects, including the laser and the structure of QD itself. The distribution of the intensity of the laser is not same through the cross section of the beam which obeys a simple Gaussian distribution. The highest intensity is in the center and the intensity is lower at the edge of the beam. Therefore, the

molecules experienced different intensities of excitation which results in a distribution in emission intensities. This effect is accounted for by measuring QDs from many different areas in the illumination area, but it can cause some distribution in observed properties. The other factor arising from the laser is related to the probability of photoexcitation. This probability depends on the angle between transition moment vector of the fluorophore and electric vector of the light. The absorption of light is maximum when the transition moment is aligned with electric vector, while the light cannot be absorbed when the transition moment is perpendicular to electric vector. Thus, not every molecule will absorb (and hence emit) equally. This effect is more important in organic molecular systems than in QDs, so the effect is expected to be minimal here. Another factor which might be responsible for this distribution was the inhomogeneity of the coating material of quantum dots. As noted in previous chapter, the uneven thickness of the coating material and drying process results in different formations of QDs which in turn results in a difference in the degree of excitation and emission of each individual molecule.

## 3.4 Batch-to-batch variability

Another batch of white quantum dots was analyzed using all of the measurements described above in order to assess reproducibility. The details of the analysis are shown in Appendix 1. The results gathered from the size distribution measurements and optical property measurements of both batches of white QDs are summarized in Table 3.1, and compared with the first batch of samples measured. From the size distribution tests, it was observed that new samples were slightly more aggregated than the original batch, with a larger intensity-weighted average size and higher polydispersity index compared with the original. However, the presence of aggregates did not have a significant influence on the optical properties. In conclusion, the second batch of

white QD showed no significant difference with the first batch excepted for a slightly higher amount of aggregation.

**Table 3.1** The results obtained from the two batches of white QD samples under the same instrument and sample preparation conditions.

| | Batch 1 | Batch 2 |
|---|---|---|
| DLS | 41 nm (PDI: 0.28) | 87 nm (PDI: 0.64) |
| AFM | 8 ± 5 nm | 6 ± 3 nm |
| TEM | 2.4 ± 0.3 nm | ---- |
| Bandgap energy | 2.53 ± 0.01eV (2.4 ± 0.1 nm) | 2.45 ± 0.01eV (2.6 ± 0.1 nm) |
| Quantum yield | 5% | 10% |
| SM fluorescence intensity | 1083 ± 274 CCD counts | 942 ± 187 CCD counts |

## 3.5 Conclusions

In this work, the optical properties of the white emitting QDs were studied at the ensemble and single molecule level, and compared with a commercial control sample. It was found that white QDs showed a relatively broad absorption spectrum indicating polydispersity and the average size derived from the band gap energy was 2.4 ± 0.1 nm, which is in good agreement with that reported by TEM in Chapter 2. The emission spectra of the white QDs showed a blue emission peak with a weaker red emission peak resulting in white light emission. The blue

emission peak was caused by the band gap emission and deep trap states on the surface were shown to be responsible for the red emission peak. It was also observed that the white QDs had a lower quantum yield of 5% in comparison with the QY of commercial QDs of 42%. From the single molecule experiments, the emission fluorescence of commercial QDs was only found in the red channel, while the emission of the white QDs was only found in the blue channel. It has been shown that the ensemble broad emission is the result of single CdSe nanocrystals which can emit over the entire "white" spectrum, instead of from a mixed population of blue and red emitters. Moreover, in agreement with the ensemble quantum yield measurements, white QDs were found to emit with lower intensity fluorescence compared to commercial QDs. Batch-to-batch variability was minimal for these samples.

# 4 Conclusions and Future Work

White light emitting semiconductor quantum dots, synthesized through aqueous chemistry under ambient conditions, have been characterized in this work to determine the mechanism of "white" fluorescence. The size measurements revealed that the resulting QDs exhibited polydispersity due to the presence of coating polymer (PAA) and had cores around 2.5 nm in diameter. The white fluorescence was the result of the combination of strong blue emission arising from the band gap emission and a weaker red emission arising from the deep trap states on the surface. It was also observed that the quantum yield of white QDs was lower in comparison to commercial QDs with a narrow emission spectrum. Single molecule fluorescence measurements were carried out using a home-built microscope to explore the behavior of single quantum dots. Compared with commercial QDs, there were no red-emitting QDs in the white QDs sample which proved that the samples were not mixture of different color emission QDs.

With the superior optical properties of high photostability, these materials can be used to build light-emitting diodes which have the potential to replace traditional incandescent and fluorescent lamps. In preliminary attempts, white QDs in chloroform were used to fabricate thin films and light emitting diodes by spin-coating. The device assembled layer-by-layer was placed in a custom-built plastic holder and each pixel was tested for the electro-optical properties under an additional voltage ranging from 0 to 15 V. While emission was observed for some devices, they emitted light for only a very short period before short-circuiting, and further study is needed to explore the best conditions for fabrication of LEDs. This observation might be attributed to several possible factors, in terms of the thick polymer layer that surrounds the semiconductor, thickness of each layer, impurities and choice of cathode material. Polymer removal might be achieved through plasma treatment without significant change to the optical properties of the

QDs. For the emission spectra, the spectrum of white QDs deposited in a film did not differ significantly from the one dispersed in solution, which indicates that the color output could be maintained when fabricated into LEDs. Therefore, this kind of white QDs are a good candidate in solid state applicants though significant improvements in device functionality and efficiency are required in the future work.

For single molecule studies, it was found that individual QDs exhibited flickering between on and off states which suppress the overall emission efficiency. Further studies of photoblinking as a function of different experimental conditions are required in order to improve the overall efficiency of fluorescence emission. Flickering / blinking in single-molecule experiments depends strongly on the excitation intensity and different coatings surrounding the semiconductor.[65,67] To explore these effects further, carrying out experiments at different excitation intensities is required. White QDs might show different rates of photoblinking, providing insight into the role that excitation plays in driving blinking dynamics. Moreover, the surface conditions have a significant influence on the photophysical properties due to the high surface-to-volume ratio.[66] The enhancement of fluorescence emission efficiency should be observed by adjusting the thickness of a shell of ZnS and varying capping ligands attached to the surface of QDs. However, the improvements of overall emission efficiency should not eliminate the deep trap states responsible for the white emission, which will be the principal challenge in the future work.

It has been shown that quantum dots can play a useful role in optimizing the photon conversion efficiency of dye-sensitized photovoltaic devices by amplifying photon collection in the visible range because of their broad absorption spectrum.[68] The white QDs investigated in this thesis might be useful in these types of applications. In order to use a semiconductor as a

mediator in solar cells, several further studies are important. Prior to the fabrication of dye-sensitized solar cells (DSSC), white QDs might be functionalized with another surface ligand to make them disperse well in electrolyte, meanwhile, to verify the optical properties with the new capping ligand and the stability in the presence of ions is also necessary. To confirm the application of white QDs as a mediator, the external quantum efficiency (EQE) measurements should be performed through the collection of current and voltage measurements for I-V curves. Furthermore, the mechanism of energy transfer from QD to sensitizer dye should be determined in order to enhance cell efficiency.

## References


(1) Dong, W.; Shen, H.-B.; Liu, X.-H.; Li, M.-J.; Li, L.-S. Spectrochimica Acta Part A: Molecular and Biomolecular Spectroscopy **2010**, 78, 537-542.

(2) Rombach-Riegraf, V.; Oswald, P.; Bienert, R.; Petersen, J.; Domingo, M. P.; Pardo, J.; Gräber, P.; Galvez, E. M. Biochemical and Biophysical Research Communications **2012**, 430, 260-264.

(3) Brus, L. E. The Journal of Chemical Physics **1984**, 80, 4403-4409.

(4) Baskoutas, S.; Terzis, A. F. Journal of Applied Physics 2006, 99, 013708.

(5) Changyu, S. International Society for Optics and Photonics 2008; In Photonics, Devices, and System IV Vol. 7138, p 71382E-71382E-6.

(6) Medintz, I. L.; Uyeda, H. T.; Goldman, E. R.; Mattoussi, H. Nature Material **2005**, 4, 435-446.

(7) Li, J.; Zhu, J.-J. Analyst **2013**, 138, 2506-2515.

(8) Jamieson, T.; Bakhshi, R.; Petrova, D.; Pocock, R.; Imani, M.; Seifalian, A. M. Biomaterials **2007**, 28, 4717-4732.

(9) Barroso, M. M. Journal of Histochemistry & Cytochemistry **2011**, 59, 237-251.

(10) Smith, A. M.; Dave, S.; Nie, S.; True, L.; Gao, X. Expert Review of Molecular Diagnostics **2006**, 6, 231-244.

(11) Jaiswal, J. K.; Mattoussi, H.; Mauro, J. M.; Simon, S. M. Nature Biotechnology **2003**, 21, 47-51.

(12) Nguyen, H. T.; Pham, T. N.; Koh, K. H.; Lee, S. physical status solidi (a) **2012**, 209, 1163-1167.

(13) Schreuder, M. A.; Xiao, K.; Ivanov, I. N.; Weiss, S. M.; Rosenthal, S. J. Nano Letters **2010**, 10, 573-576.

(14) Solid-State Lighting Research and Development: Multi-Year Program Plan provided for Lighting Research and Development Building Technologies Program, Office of Energy Efficiency and Renewable Energy, U.S. Department of Energy. April 2012.

(15) Li, Y.; Rizzo, A.; Cingolani, R.; Gigli, G. Microchimica Acta **2007**, 159, 207-215.

(16) Polikarpov, E.; Thompson, M. E. Material Matters **2007**, 3, 21.

(17) Zyga, L. Quantum dot LEDs get brighter, more efficient. Phys.org. April 2012.

http://phys.org/news/2012-04-quantum-dot-brighter-efficient.html

(18) Kwak, J.; Bae, W. K.; Lee, D.; Park, I.; Lim, J.; Park, M.; Cho, H.; Woo, H.; Yoon, D. Y.; Char, K.; Lee, S.; Lee, C. Nano Letters **2012**, 12, 2362-2366.

(19) Anikeeva, P. O.; Halpert, J. E.; Bawendi, M. G.; Bulović, V. Nano Letters **2007**, 7, 2196-2200.

(20) Dukes, A. D.; Samson, P. C.; Keene, J. D.; Davis, L. M.; Wikswo, J. P.; Rosenthal, S. J. The Journal of Physical Chemistry A **2011**, 115, 4076-4081.

(21) Bowers, M. J.; McBride, J. R.; Rosenthal, S. J. Journal of the American Chemical Society **2005**, 127, 15378-15379.

(22) Baker, D. R.; Kamat, P. V. Langmuir **2010**, 26, 11272-11276.

(23) Dukes, A. D.; Schreuder, M. A.; Sammons, J. A.; McBride, J. R.; Smith, N. J.; Rosenthal, S. J. The Journal of Chemical Physics **2008**, 129, -.

(24) Rajeshwar, K.; de Tacconi, N. R.; Chenthamarakshan, C. R. Chemistry of Materials **2001**, 13, 2765-2782.

(25) Hines, D. A.; Kamat, P. V. ACS Applied Materials & Interfaces **2014**, 6, 3041-3057.

(26) Bowers II, M. J.; McBride, J. R.; Garrett, M. D.; Sammons, J. A.; Dukes III, A. D.; Schreuder, M. A.; Watt, T. L.; Lupini, A. R.; Pennycook, S. J.; Rosenthal, S. J. Journal of the American Chemical Society **2009**, 131, 5730-5731.

(27) Moerner, W. E.; Fromm, D. P. Review of Scientific Instruments **2003**, 74, 3597-3619.

(28) Zondervan, R.; Kulzer, F.; Kol'chenk, M. A.; Orrit, M. The Journal of Physical Chemistry A **2004**, 108, 1657-1665.

(29) Lakowicz, J. R. Principles of Fluorescence Spectroscopy; Second ed.; Kluwer Academic/Plenum Press: New York, 1999.

(30) Th. Basché, W. P. A., and W. E. Moerner J. Opt. Soc. Am. B **1992**, 9, 829-836

(31) Murray, C. B.; Norris, D. J.; Bawendi, M. G. Journal of the American Chemical Society **1993**, 115, 8706-8715.

(32) Chan, W. C. W.; Nie, S. Science **1998**, 281, 2016-2018.

(33) Bruchez, M.; Moronne, M.; Gin, P.; Weiss, S.; Alivisatos, A. P. Science **1998**, 281, 2013-2016.

(34) Gerion, D.; Pinaud, F.; Williams, S. C.; Parak, W. J.; Zanchet, D.; Weiss, S.; Alivisatos, A. P. The Journal of Physical Chemistry B **2001**, 105, 8861-8871.

(35) Rajh, T.; Micic, O. I.; Nozik, A. J. The Journal of Physical Chemistry **1993**, 97, 11999-12003.

(36) Bao, Y.; Li, J.; Wang, Y.; Yu, L.; Wang, J.; Du, W.; Lou, L.; Zhu, Z.; Peng, H.; Zhu, J. Optical Materials **2012**, 34, 1588-1592.

(37) Arzenšek, D.; Dynamic light scattering and application to proteins in solutions, 4th year seminar, University of Ljubljana: May 19, 2010.

(38) Malvern Instruments Ltd., Zetasizer nano series user manual-Chapter 14, United Kingdom, MAN0317, Issue 1.1, Feb 2004.

(39) Sójka-Ledakowicz, J.; Olczyk, J.; Sielski, J. Fibres & Textiles in Eastern Europe **2011**, 19, 85.

(40) Siwińska-Stefańska, K.; Krysztafkiewicz, A.; Jesionowski, T. Fizykochemiczne Problemy Mineralurgii **2008**, 42, 141-152.

(41) Malvern Instruments Ltd., Dynamic light scattering common terms defined. United Kingdom, Inform whitepaper, version 1, **2011**.

(42) Wilczura-Wachnik, H., Polymer and biomaterials laboratory, Manual for experiment "Dynamic Light Scattering application in size detection of molecules and molecular aggregates", University of Warsaw, Faculty of Chemistry, Chemical Technology Division.

(43) McNeil, S. E.; Grobelny, J.; DelRio, F.; Pradeep, N.; Kim, D.-I.; Hackley, V.; Cook, R. In Characterization of Nanoparticles Intended for Drug Delivery; Humana Press: 2011; Vol. 697, p 71-82.

(44) Hoo, C.; Starostin, N.; West, P.; Mecartney, M. Journal of Nanoparticle Research **2008**, 10, 89-96.

(45) Starostina, N.; West, P. Part II: Sample Preparation for AFM Particle Characterization. Pacific Nanotechnology Inc., Santa Clara, CA, 2006: p. 1-10..

(46) Lee, J.; Yang, B.; Li, R.; Seery, T. A. P.; Papadimitrakopoulos, F. The Journal of Physical Chemistry B **2006**, 111, 81-87.

(47) NANOCOMPOSIX. Guidelines for Dynamic Light Scattering Measurement and Analysis. 2012 [cited; Available from: NANOCOMPOSIX.COM].

(48) Rao, A.; Schoenenberger, M.; Gnecco, E.; Glatzel, T.; Meyer, E.; Brändlin, D.; Scandella, L. In Journal of Physics: Conference Series; IOP Publishing: 2007; Vol. 61, p 971.

(49) Klapetek, P.; Valtr, M.; Necas, D.; Salyk, O.; Dzik, P. Nanoscale Research Letters **2011**, 6, 514.

(50) Dobrovolskaia, M. A.; Patri, A. K.; Zheng, J.; Clogston, J. D.; Ayub, N.; Aggarwal, P.; Neun, B. W.; Hall, J. B.; McNeil, S. E. Nanomedicine: Nanotechnology, Biology and Medicine **2009**, 5, 106-117.

(51) Cheng, C.; Yan, H. Physica E: Low-dimensional Systems and Nanostructures **2009**, 41, 828-832.

(52) Zhang, Y.; Shakouri, A. Properties of Materials Laboratory, manual for experiment "Optical Absorption", Electrical Engineering Department, University of California at Santa Cruz, May 2002.

(53) Weber, M. H.; Lynn, K. G.; Barbiellini, B.; Sterne, P. A.; Denison, A. B. Physical Review B **2002**, 66, 041305.

(54) González-Borrero, P. P.; Sato, F.; Medina, A. N.; Baesso, M. L.; Bento, A. C.; Baldissera, G.; Persson, C.; Niklasson, G. A.; Granqvist, C. G.; Ferreira da Silva, A. Applied Physics Letters **2010** 96, 061909.

(55) Dabbousi, B. O.; Rodriguez-Viejo, J.; Mikulec, F. V.; Heine, J. R.; Mattoussi, H.; Ober, R.; Jensen, K. F.; Bawendi, M. G. The Journal of Physical Chemistry B **1997**, 101, 9463-9475.

(56) Vinayakan, R.; Shanmugapriya, T.; Nair, P. V.; Ramamurthy, P.; Thomas, K. G. The Journal of Physical Chemistry C **2007**, 111, 10146-10149.

(57) Kamat, P. V. Chemical Reviews **1993**, 93, 267-300.

(58) Smith, A. M.; Nie, S. Accounts of Chemical Research **2009**, 43, 190-200.

(59) Chandramohan, S.; Ryu, B. D.; Kim, H. K.; Hong, C.-H.; Suh, E.-K. Optics Letters **2011**, 36, 802-804.

(60) Fischer, M.; Georges, J. Chemical Physics Letters **1996**, 260, 115-118.

(61) Peterson, J. J.; Nesbitt, D. J. Nano Letters **2008**, 9, 338-345.

(62) Galland, C.; Ghosh, Y.; Steinbruck, A.; Sykora, M.; Hollingsworth, J. A.; Klimov, V. I.; Htoon, H. Nature **2011**, 479, 203-207.

(63) Krauss, T. D.; Peterson, J. J. Nat Mater **2012**, 11, 14-16.

(64) Wang, X.; Ren, X.; Kahen, K.; Hahn, M. A.; Rajeswaran, M.; Maccagnano-Zacher, S.; Silcox, J.; Cragg, G. E.; Efros, A. L.; Krauss, T. D. Nature **2009**, 459, 686-689.

(65) Nirmal, M.; Dabbousi, B. O.; Bawendi, M. G.; Macklin, J. J.; Trautman, J. K.; Harris, T. D.; Brus, L. E. Nature **1996**, 383, 802-804.

(66) Yuan, C.-T.; Chou, W.-C.; Chen, Y.-N.; Chou, J.-W.; Chuu, D.-S.; Lin, C.-A. J.; Li, J. K.; Chang, W. H.; Shen, J.-L. The Journal of Physical Chemistry C **2007**, 111, 15166-15172.

(67) Li, L.; Tian, G.; Luo, Y.; Brismar, H.; Fu, Y. The Journal of Physical Chemistry C **2013**, 117, 4844-4851.

(68) Adhyaksa, G. W. P.; Lee, G. I.; Baek, S.-W.; Lee, J.-Y.; Kang, J. K. Sci. Rep. **2013**, 3.

## Appendix 1 :

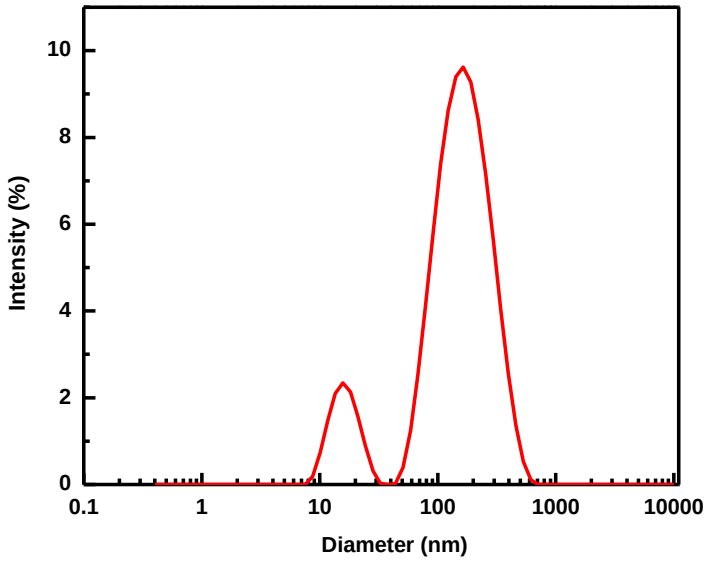


Figure A-16. Analysis of nanocrystal size by DLS. The size distribution was shown by intensity and the Z-average diameter is 87 nm with a polydispersity index of 0.64.

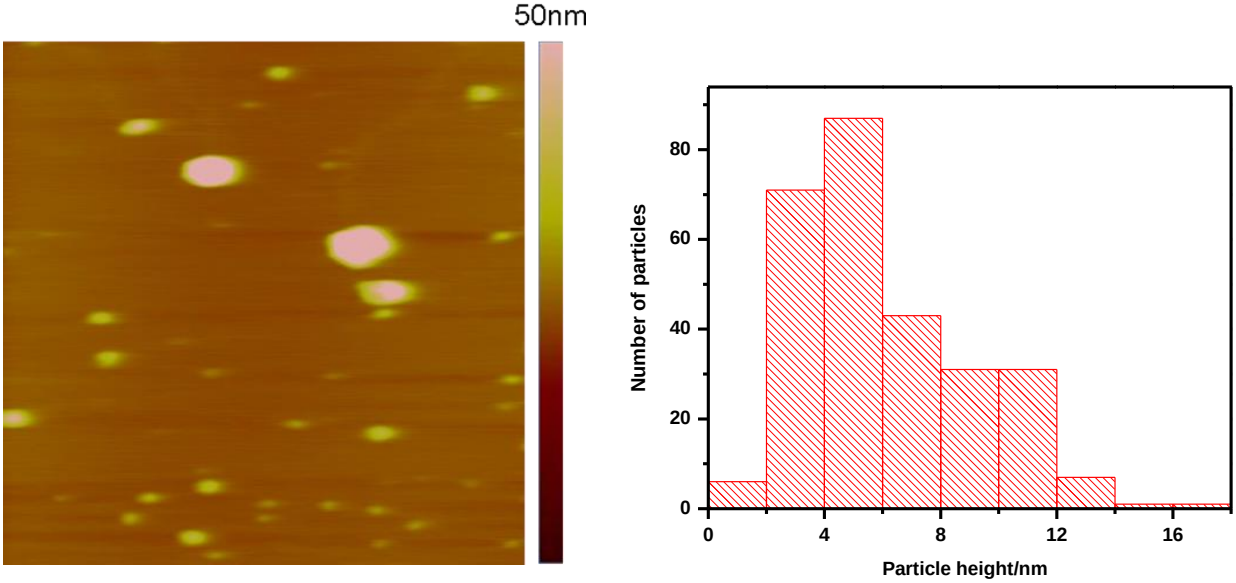


Figure A-17. AFM height image (2 μm x 2 μm) and histogram of size distribution (278 quantum dots were measured). The average size was 6 ± 3 nm.

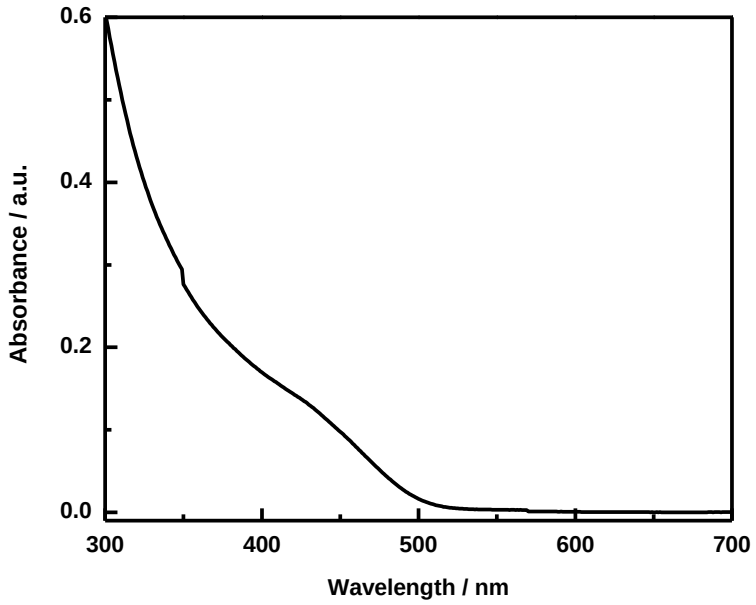


Figure A-18. Absorption spectrum of white QDs. The cut off wavelength of the white QD was 506 nm with an uncertainty of 3 nm which yield a band gap of 2.45 ± 0.01 eV. Based on the model developed by Baskoutas's group, we estimated the average core diameter of white QD was 2.6 ± 0.1 nm

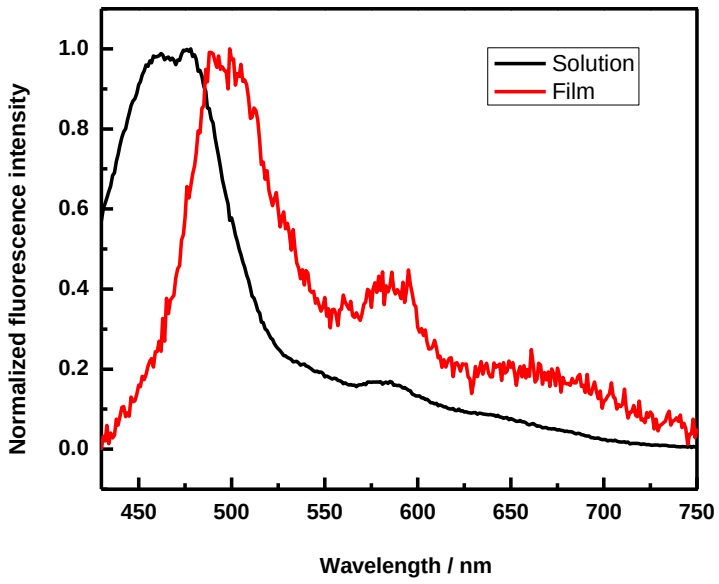


Figure A-19. Photoluminescence spectra of white QDs in solution (black line) and thin film (red line).

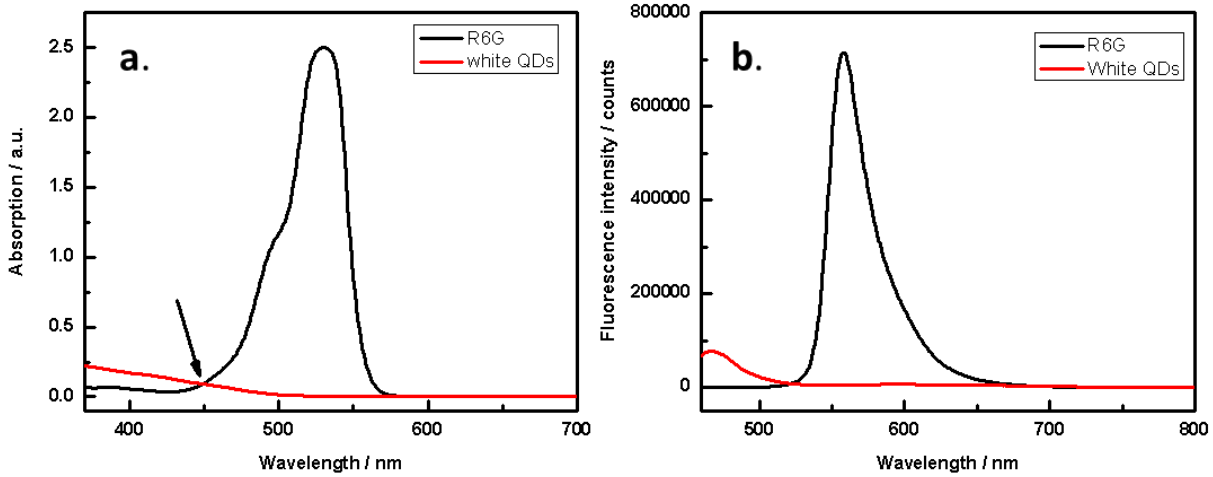


Figure A-20. The absorption (a) and emission (b) spectra of R6G (black line) and white QDs (red line). The arrow points at the matched wavelength which was used for excitation. At the same excitation wavelength of 450 nm, the emission spectra of R6G and white QDs were obtained in the range from 460 nm to 800 nm and the calculated quantum yield was 10%.

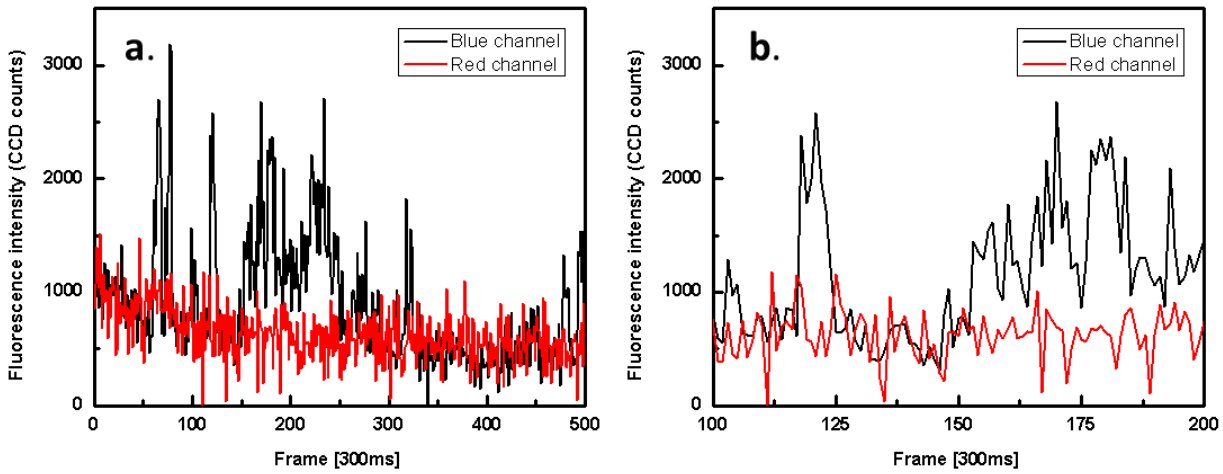


Figure A-21. (a) Typical single molecule fluorescence time trajectories of a white QD. (b) 100 frames of the total 500 frames in (a). Measurements were done at 0.2 kW/cm$^2$ illumination intensity. The intensity of the individual QD in each frame of both channels was measured in an area of 4 x 4 pixels (400 nm x 400 nm).

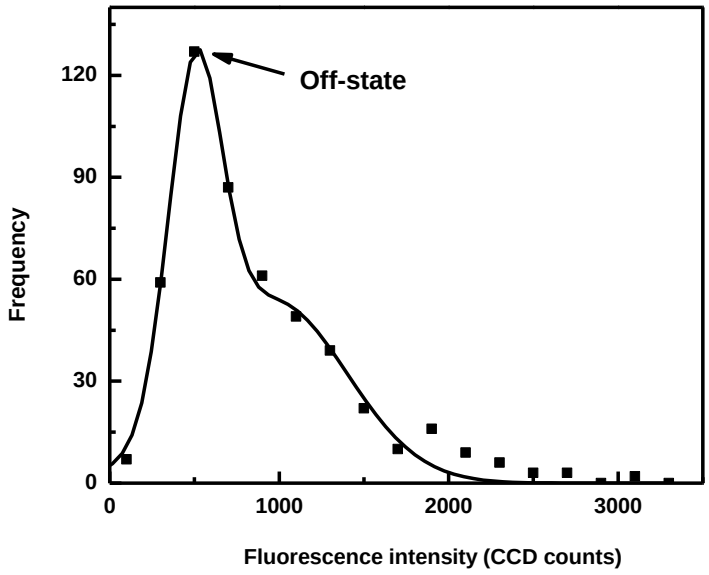


Figure A-22. Frequency of fluorescence intensity histogram fitted with two Gaussian peaks.

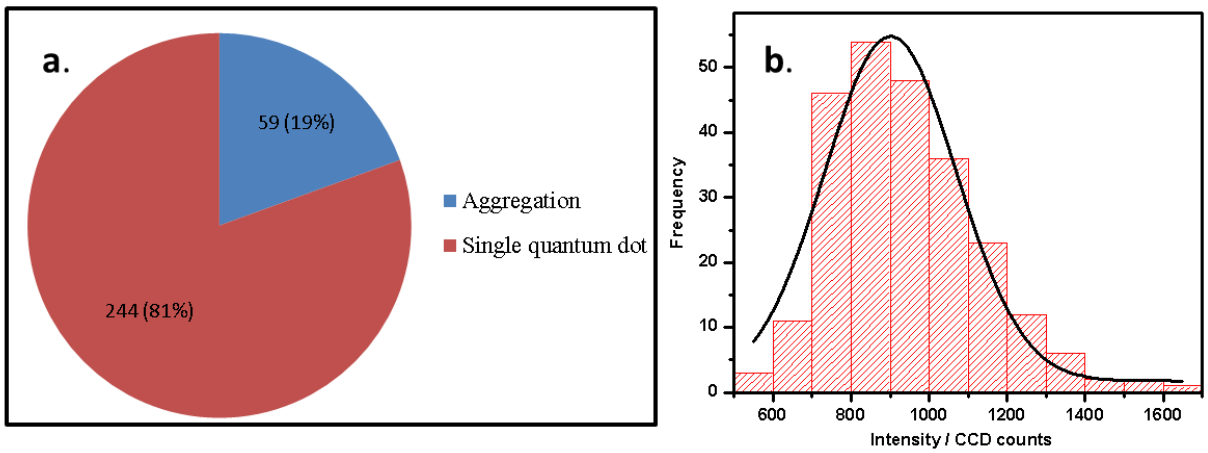


Figure A-23. (a) Pie chart showing distributions of different types particles for white QD sample. (b) Histograms of single-molecule fluorescence intensities. The distribution shows an approximately Gaussian distribution and the average on-state intensity was 942 ± 187 CCD counts. The excitation intensity was 0.2 kW/cm$^2$.